SYNOPTIC TRANSPORT MODELING IN THE CA RIVER BASIN, NORTH CENTRAL VIETNAM

Ho Thi Phuong

Graduate School of Environmental and Life Science
(Doctor's Course)

OKAYAMA UNIVERSITY

September 2019

TABLE OF CONTENTS

Page

LIST OF FIGURES

LIST OF TABLES

ABSTRACT

The study was performed in the Ca River basin, which is the third largest river in north-central Vietnam, located between 18°15′00″N and 20°10′30″N and 103°45′20″E and 105°15′20″E. Ca River basin covers an area of 27,200 km^2 in which the area in Vietnam territory is 17,730 km^2, holding 65.2% of the total drainage area. The trunk river length is 531 km, of which 170 km runs through Lao PDR and 361 km runs through Vietnam. Ca River, like many other rivers around the world, have been impacted by economic development. Various sized reservoirs have been constructed along the rivers for power generation, water supply, and flood control. In addition, other anthropogenic activities (e.g., intensive agriculture, land-use change, and industrial development) may disrupt the dynamic equilibrium between the movement of water and the movement of sediment that exists in free-flowing rivers, resulting in an alteration of natural river regimes, a modification of a river's morphology and riverbed characteristics, and a change in ion constitution. The aim of dissertation thesis is to examine the degree of human-induced alteration of the natural flow regime and the material budgets in the Ca River basin using Synoptic model include the Tank model, regime law and resistance law.

The Hieu River is the largest tributary on the left bank of the Ca River. Here, we use cumulative anomaly tests and Pettitt tests to ascertain the turning points in annual rainfall and discharge during the time period 1962–2014. The results of our statistical analysis reveal a breaking point in 1982 for the rainfall time series and in the late 1970s and late 1990s for the discharge time series. A storage-type hydrological model is used to determine runoff processes for different periods corresponding to detecting points of rainfall and discharge. The results of our model simulation confirm that a two-tank model with monthly input data is the most appropriate tank model for the Hieu River. The difference between the hydrographs improved when we used a rain factor as a function of the month. A comparison between the observed and calculated runoff revealed a drastic decrease between 1999 and 2014. The rate of discharge loss in the Lower Basin was approximately six times higher than that in the Upper Basin, a finding potentially due to reservoir construction and intensive water use for agricultural and residential purposes.

The river regime laws of the hydraulic properties of the cross sections of two hydrological stations (Dua and Yen Thuong) along the Ca River were combined into power functions with exponents of 1.46–1.85 using the Manning roughness coefficient and the

settling velocity or the particle size to simulate the suspended sediment load. The Nash-Sutcliffe efficiency, percent bias, and the ratio of the root-mean-square error to the standard deviation of the measured data were used to evaluate the calibration process for the pre-dam period (1994–2004) and for validation for the post-dam period (2005–2014). Effects of dam construction include a change in the relationship between the Manning roughness coefficient and sediment particle size. The observed sediment load decreased by approximately 20–40% after dam construction at both stations. We used a power function with exponents of 0.968 and 0.992 for the dissolved solid load to calculate the long-term annual total dissolved solids at the Dua and Yen Thuong stations, respectively. After dam construction, the average value of the total suspended solids-to-total dissolved solids ratio decreased from 3.0 to 2.3 at the Dua station and from 4.1 to 2.2 at the Yen Thuong station.

This study investigates the chemical composition of dissolved loads in the Ca River basin. The water samples were collected for 1 year from August 2017 to July 2018 at three hydrological stations located in the mainstream of the Ca River. We found that carbonate weathering is the dominant process controlling the water chemistry in the study area. Bicarbonate and calcium are dominant chemical species, accounting for 84.4% and 62.0% of the total anionic and cationic charge, respectively. The average dissolved-solids concentration is 144 mg/l and generally decrease from the upstream to downstream, resulting in a decrease of the major ions in the downstream basin. The variation of major chemical ions and suspended solids concentration with discharge was also investigated. As a result, major chemical weathering products behave chemostatically, with increasing discharge in the upstream. However, the dilution behavior of solutes is shown in the midstream and downstream. The ion species of NO_3^- and PO_4^{3-} show constant to increasing concentration in the drainage basin, indicating the additional sources of organic degradation and human activities. There is primary evidence that water storage for the reservoirs has impacted on a variation of suspended solids and dissolved solids in the Ca River.

CHAPTER 1. CA RIVER BASIN

1.1. NATURAL CHARACTERISTICS

1.1.1. Topographic

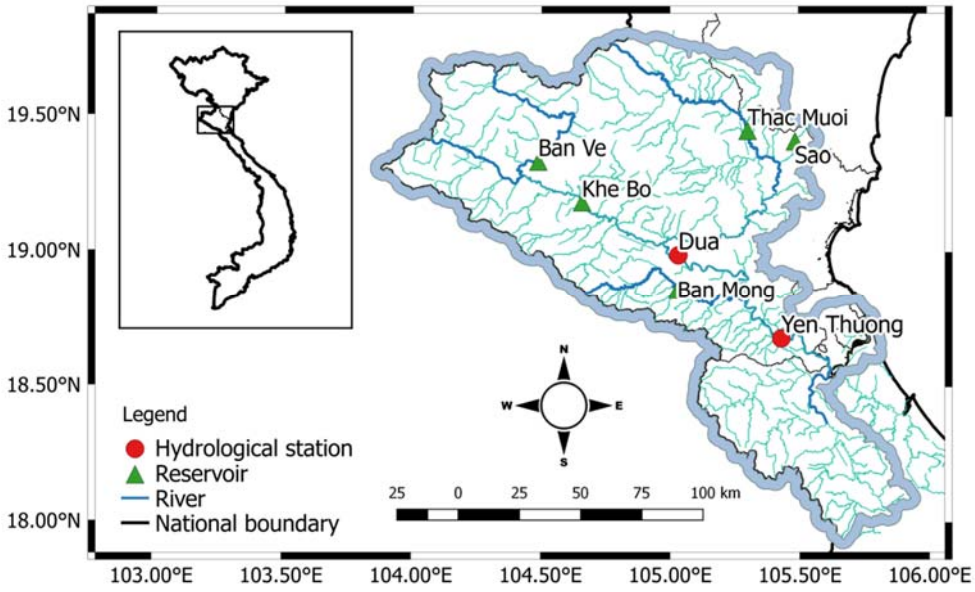

Figure 1.1. Ca River basin

The Ca River basin is an international river, located between 18º15'00"N to 20º10'30"N and 103º45'20"E to 105º15'20"E (Figure1.1). The basin covers an area of 27,200 km^2, including 17,730 km^2 in Vietnam's territory and 9470 km^2 in Laos. The main river originates from Mt. Muong Khut and Muong Lap at an elevation of 1800 to 2000 m in Laos. The river enters into the NgheAn province at Keng Du and flows to the Eastern Sea at the Cua Hoi estuary. The Ca River bed is very narrow, with steep slopes in the upstream area, it then widens up in the middle basin (from Con Cuong to Anh Son), and finally joins the Hieu River on its left side. In the downstream area, the Ca River flows through the plain and joins the La River on the right side.

The entire upstream in Lao PDR has an average altitude of over 1000 meters. In Vietnam, more than 80% of the basin area is mountainous. The length of the main Ca river is 531 km in total, of which 361 km is in Vietnam and its mean elevation is 294 m a.s.l. .

Hieu River is the largest tributary on the left side of the Ca River. The catchment area of the Hieu River is 5340 km^2, its length is 228 km and originates from Pu Hoat Range in the Laos Vietnam boundary. This then flows into the Ca River at Anh Son.

La River is the main tributary on the right side of the Ca River: it originates from the Giai mountainous area and enters into Ca river at Cho Trang. The catchment area of the La River is 3210 km^2.

Picture 1.1. Midstream of Ca river

(Taken in Dua hydrological station on June 28, 2016)

1.1.2. Vegetation cover and soil

According to the land survey in 2010, the structure of the land on the Vietnam territory is as follows:

- 1,418,053 ha of agricultural land
- 1,085,897.9 hectares of forestry land
- 158,518,4 ha of non-agricultural land
- 386,092 ha of unused land.

The vegetation cover on agricultural land is estimated to be at 20–25%. Forests in the Ca River basin are largely located in the upstream of three Laos provinces (Bolikhamxay, XiengKhouang, and Houaphanh). In Vietnam, the forest is concentrated in the north, northwest, and southwest of the basin at an elevation of 150 to 1500 m (IWRP 2012). The natural land is mostly evergreen and semi deciduous tropical forest, although mixed forests can be found in some areas (Giang et al. 2014).

Before 1995 the forest in the Ca river basin was rapidly reduced due to exploitation and poor maintenance. According to the forest inventory data of the Ca River basin in Vietnam, in 1943 there was about 1.2 million ha of forest and in 1999, the forests were only about 710,000 ha. The coverage was 35.5%. From 1995 to 2010 the forest in the basin has started to be preserved and restored due to rapid forest plantations and land and forest

allocation. This combined with the mountainous economic development programs has made the current forest in Nghe An rise to 51.5% coverage and Ha Tinh has reached 50.2%.

The soil in this area is formed from parent rocks, mainly Ferralsol accounting for 83.51% (IWRP 2012; Nauditt and Ribbe 2017). Other soil types are Fluvisol and Acrisol.

Picture 1.2. Forest cover in moutainous area of Ca river

(Taken in My Ly catchment on August 13, 2017)

1.1.3.Climate

a/ Temperature

Table 1.1. Average temperture of many years in the Ca River

Stations	Months												Ave
	Jan	Feb	Mar	Apr	May	Jun	Jul	Aug	Sept	Oct	Nov	Dec	(ºC)
Con Cuong	17.1	18.0	20.4	24.5	27.0	28.1	27.7	27.2	25.9	23.2	20.2	18.4	23.1
Cua Rao	16.9	18.9	21.7	25.0	26.8	27.5	27.1	26.7	25.7	23.6	20.0	17.7	23.1
Do Luong	17.8	18.5	20.9	24.5	27.5	29.1	29.1	28.1	26.7	24.5	21.6	18.8	23.9
Ha Tinh	16.7	17.7	20.4	24.5	27.1	28.8	28.8	27.0	25.4	23.8	20.9	18.4	23.3
Huong Khe	19.2	20.1	22.4	25.9	28.5	29.7	29.6	29.3	27.4	25.3	22.8	20.2	25.0
Huong Son	17.2	17.9	20.4	24.3	27.8	29.5	29.4	28.9	27.8	25.4	22.2	18.8	24.1
Kim Cuong	16.2	17.3	19.9	23.9	27.6	29	28.9	28.5	27.4	24.8	21.6	18.3	23.6
Ky Anh	18.0	19.5	21.4	25.2	27.8	30.4	30.1	28.8	27.0	25.4	22.3	19.4	24.6
Quy Chau	15.2	17.2	19.7	23.9	26.0	26.9	27.0	26.2	25.1	23.1	19.2	15.4	22.1
Quy Hop	17.9	19.1	21.6	25.2	27.4	28.5	28.9	27.9	26.4	24.6	21.6	18.6	24.0
Quynh Luu	17.1	18.0	19.9	23.4	26.7	28.1	28.4	27.4	26.2	23.3	19.8	18.4	23.1
Tay Hieu	17.0	18.1	20.7	24.5	27.2	28.6	28.7	27.6	26.3	24.0	21.0	17.9	23.5
Vinh	17.6	18.2	20.6	24.2	27.8	29.6	29.7	28.7	26.9	24.6	21.8	18.8	24.0

The Ca River basin is located in a monsoon climate, with two distinct seasons: the wet and dry seasons. The wet season, starting from May to October, is hot and humid due to the southwest monsoon (locally called the Laos wind). The dry season lasts six months from November to April which is cold and dry caused by the northeast monsoon. The temperature of the plain is higher than the midland and mountainous areas. This is shown in the average temperature of Vinh 23.8ºC, Do Luong 23.7ºC, Tuong Duong 23.6ºC and Tay Hieu 23.2ºC (Table 1.1).

b/ Humidity

The annual average humidity in the Ca River basin ranges from 82% to 85%. Humidity corresponds to the evaporation of the year. The middle of the basin with high humidity corresponds to low evaporation, and mountainous areas and the plain has high evaporation corresponding to low humidity. The highest monthly humidity reach up to 94% in January and February, the lowest humidity is in July (Table 1.2).

Table 1.2. Average humidity of many years in the Ca River

Stations	**Months**												**Ave**
	Jan	Feb	Mar	Apr	May	Jun	Jul	Aug	Sept	Oct	Nov	Dec	**(%)**
Con Cuong	88.2	88.6	87.7	84.8	81.3	79.7	78.3	83.7	86.7	88.1	87.3	87.4	85.2
Cua Rao	81.7	80.5	79.5	78.7	78.9	80.6	80.7	84.1	85.6	85.8	85.1	83.3	82.0
Do Luong	86.9	88.4	88.9	86.9	82.4	79.2	78.8	83.6	86.5	85.9	85	84.9	84.7
Ha Tinh	88.8	90.3	90.1	85.7	79.9	74.6	73.6	79.3	85.4	87.4	87.3	87.8	84.2
Huong Khe	88.9	89.6	89.3	85.3	81.2	77.0	74.8	82.1	86.8	88.9	87.9	87.8	85.0
Huong Son	90.0	90.5	89.7	87.3	82.4	76.3	76.6	81.2	85.5	89.0	87.8	87.2	85.3
Kim Cuong	88.9	89.6	89.3	85.3	81.2	77.0	74.8	82.1	86.8	88.9	87.9	87.8	85.0
Ky Anh	91.2	92.0	90.7	87.1	80.8	71.2	70.3	77.1	85.5	87.4	86.9	87.5	84.0
Quy Chau	87.0	86.3	86.1	84.7	83.6	85.1	84.8	87.8	88.5	88.0	87.2	87.2	86.4
Quy Hop	84.5	85.5	85.0	83.0	81.9	79.1	79.6	85.5	86.7	86.1	82.9	83.8	83.6
Quynh Luu	85.5	87.8	89.7	89.1	84.1	77.8	80.1	84.9	86.2	84.3	82.9	83.6	84.7
Tay Hieu	87.4	87.2	86.5	84.6	83.5	83.8	83.7	87.4	88.1	88.1	87.1	86.9	86.2
Vinh	74.9	73.9	79.9	85.8	86.6	84.8	85.5	87.2	88.5	88.6	85.8	79.4	83.4

c/ Rainfall

Mean annual precipitation in the basin ranges from 1100 mm in the upstream mountain area to 2400 mm close to the junction with the La river. The average rainfall of the whole basin is 1800 mm. Rainfall is concentrated in one rainy season from May to October when falls 80% to 85% of annual rainfall. The heaviest rainfall occurs around September

when the mean of the maximum daily rainfall is up to 250 mm in the coastal area, and in 2010 a maximum value up to 800 mm was recorded in 24 hours (Table 1.3).

Table 1.3. Average rainfall of many years in the Ca River

Stations	Months												Ave
	Jan	Feb	Mar	Apr	May	Jun	Jul	Aug	Sept	Oct	Nov	Dec	(mm)
Muong Xen	7	6	26	74	158	144	155	231	201	114	19	5	1142
Cua Rao	11	14	33	80	158	157	153	226	227	150	35	11	1254
Con Cuong	34	36	50	86	183	146	164	263	337	294	77	31	1700
Dua	29	36	48	85	186	137	152	264	377	323	90	34	1760
Do Luong	32	32	42	84	161	133	149	262	391	371	100	36	1792
Cho Trang	41	33	41	62	125	122	97	216	464	552	179	70	2003
Huong Khe	42	45	62	95	215	160	151	294	457	577	188	75	2360
Hoa Duyet	63	51	59	82	209	135	138	290	487	575	198	94	2379
Quy Chau	16	14	29	85	225	206	196	290	322	227	54	18	1681
Tay Hieu	22	22	31	69	155	160	175	273	340	282	58	22	1609
Vinh	26	27	38	66	140	126	116	246	411	428	110	40	1774

1.2.SOCIO-ECONOMIC CHARACTERISTICS

In this part of Vietnam the population is 3,557,963 people with a natural area of 19,626 km^2 (in 2010). Population is mostly concentrated in cities, towns, and delta areas such as Vinh city, Cua Lo town, Hong Linh town and other smaller town. The population of Ca River basin is unevenly distributed. In the highlands and mountainous areas it is sparsely populated while the urban areas and the plains have high density populations. The average population density is 175 people/km^2. The highest population density is 2912 people/km^2 in Vinh city. Following that is 1851 people/km^2 in Cua Lo town. The lowest density is 25 people/km^2 in Tuong Duong district.

The total number of laborers in the whole region by 2010 is around 2,265,580 people. In particular, laborers in the agriculture - forestry - fishery account for about 65%. Laborers in the industry and construction sectors account for approximately 12%. Laborers working on service, trade, education sectors account for about 23% of laborers.

Laborers in the age group of 20–40 account for about 30–35%, laborers in the age of 40–60 account for about 20%.

The main economy in the basin still uses agriculture as a foundation for development, but the economic structure has made positive changes in recent years. The proportion of

industry and service is increasing, the proportion of agriculture in the economy tends to decrease.

1.3.RUNOFF AND RESERVOIRS

1.3.1.Runoff

The total annual average water volume of the drainage basin is 23.3 billion m^3, this corresponds to the average annual discharge of 738 m^3/s. The water volume that flows in Vietnam is 17.5 billion m^3, and in Laos 5.8 billion m^3 of water.

Floods on Ca River have 2 distinct periods: minor floods occur in May and June and the main flood occurs in September, October and November. Floods on the Ca River's main stream and tributaries appear not at the same time.

- In the main stream of the upstream of Ca River, the flood season occurs from June to the end of October (Table 1.4)
- In the middle part from Dua to Yen Thuong, the flood season starts from June and ends in November
- In Hieu river, the flood season starts from August and ends in November
- In La river, the flood season starts from August or early September and ends later in December.

Table 1.4. The annual flow of many years at selected stations in the Ca River

Station	River	Area (km^2)	Water volumne (10^9 m^3)	Discharge (m^3/s)
Muong Xen	Nam Mo	2,620	2.12	67.2
River mouth	Nam Mo	3,930	3.00	95.8
Cua Rao	Ca	12,800	6.72	213
Dua	Ca	20,800	12.93	410
Yen Thuong	Ca	23,000	16.65	528
Quy Chau	Hieu	1,500	2.50	79.4
Nghia Khanh	Hieu	4,020	3.94	125
River mouth	Hieu	5,340	5.24	166
Thac Muoi	Giang	785	1.15	36.4
River mouth	Giang	1,050	1.49	47.2
Son Diem	Ngan Pho	790	1.54	48.9
River mouth	Ngan Pho	1,060	2.00	62.3
Hoa Duyet	Ngan Sau	1,880	3.53	112
River mouth	River mouth	3,210	5.90	187
River mouth	Total basin	27,200	23.30	738

1.3.2.Reservoirs

Many reservoirs have been built in the Ca River basin: the reservoirs of Ban Ve and Khe Bo on the main stream of the Ca River, the Ban Mong reservoir on the Hieu River, and the Sao River reservoir located in a tributary of the Hieu River (Table 1.5). The operation of these reservoirs, which have a total storage capacity of 2.8×10^9 m^3, an installed power generation capacity of 485 MW (excluding Song Sao) has to meet flood control with 411×10^6 m^3 storage available, hydropower generation, water supply for irrigating 33,487 hectares, industrial, domestic and environmental demand.

Table 1.5. Major reservoirs in the Ca River (Chikamori et al. 2012)

Name of dam (reservoir)	Catchment area (km^2)	Gross capacity (10^6 m^3)	Effective capacity (10^{6e} m^3)	Year of construction	Year of completion
Ban Ve	8,700	1834.6	1383	12/2005	2009
Ban Mong	2,785	252.6	125.8	5/2010	2012
Khe Bo	14,300	97.8	17.2	10/2007	12/2010

Picture 1.3. Ban Ve reservoir (Source: http://kttvqg.gov.vn)

REFERENCES

Chikamori H, Heng L, Daniel T (eds) (2012) Catalogue of rivers for Southeast Asia and the Pacific–Volume VI. UNESCO-IHP Regional Steering Committee for Southeast Asia and the Pacific. http://unesdoc.unesco.org/images/0021/002170/217039e.pdf

IWRP (2012) Synthesis report of "Review of water resources planning in the Ca River basin" (in Vietnamese). Institute of Water Resources Planning, Directorate of Water Resources, Ha Noi

Giang PQ, Toshiki K, Sakata M, Kunikane S, Vinh TQ (2014) Modelling climate change impacts on the seasonality of water resources in the upper Ca river watershed in Southeast Asia. Scientific World Journal, 2014. http://doi.org/10.1155/2014/279135

Nauditt A and Ribbe L (eds) (2017) Land use and climate change interactions in central Vietnam. Springer Book Series: Water Resources and Development

CHAPTER 2. SYNOPTIC MODEL

Like many other rivers around the world, Ca River has been impacted by economic development. Various sized reservoirs have been constructed along the rivers for power generation, water supply, and flood control. In addition, other anthropogenic activities (e.g., intensive agriculture, land-use change, and industrial development) may have disrupted the dynamic equilibrium between the movement of water and the movement of sediment that exists in free-flowing rivers. The aim of this dissertation thesis is to examine the degree of human-induced alteration to the natural flow regime and the material budget in the tributaries and the mainstream of the Ca River basin using the **Synoptic Model**.

The synoptic model consists of four parts, including configuration, hydrological, hydraulic, and operational parts. The configuration of the river basin is described by stream order theories by Strahler (1957), Shreve (1966), and Scheidegger (1968).

Firstly, the dependent variables are number, average bed slopes, average drainage area, average length of each stream order and the independent variable in the stream order.

Secondly, the regime law was shown by Leopold & Maddock (1953), where the width, depth and mean velocity of a cross-section is described by the local discharge. The regime laws are used in Chapter 4 and dimensional consideration was added.

Thirdly, as resistance laws, the friction velocity and the average velocity formulas of uniform flows are estimated as functions of the depth or hydraulic radius. The friction velocity is an essential parameter for sediment hydraulics in Chapter 4.

The last law is the Kirchhoff's to denote continuity at a confluence, a distributary and storage and release of a reservoir including water quality at conjunction. However, the configuration of the river basin and the Kirchhoff's are not investigated in this study.

The equations for n and ks are the mean velocity formulas however the velocity is given by the regime law and the closure is made. The discharge should be provided by a runoff model, and it is calculated by the hydrological tank model (as shown in Chapter 3) by the water quality routine as dissolved matters (as shown in Chapter 4 and Chapter 5). It is the form of loading equations (L-Q) of both dissolved and particulate matters, respectively. Rating curve of water level and discharge equation (H-Q) with the duration curve of discharge ordering is all possible by using the tank model.

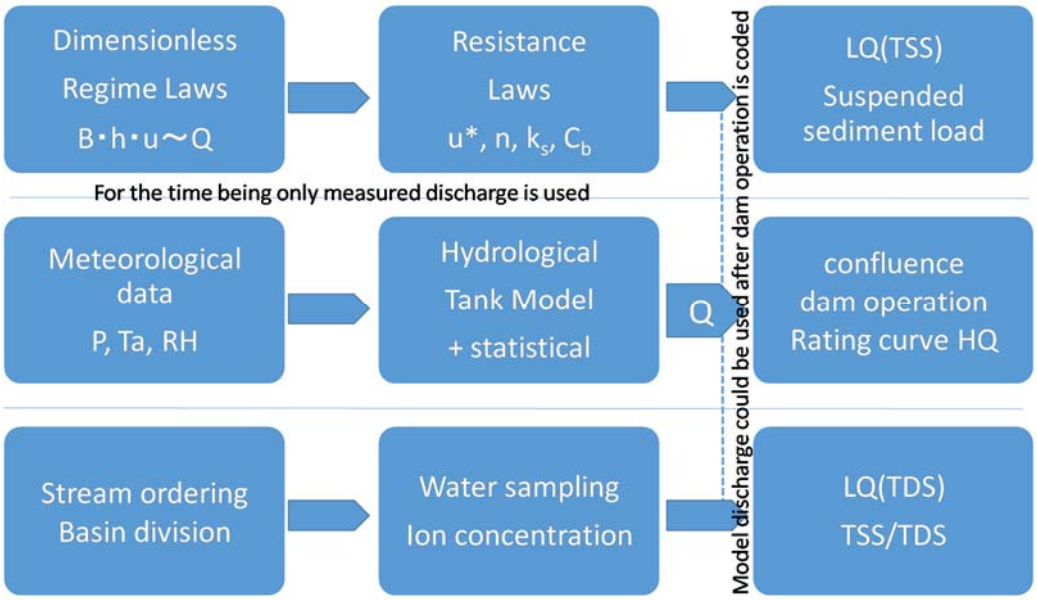

Figure 2.1. Synoptic model

REFERENCES

Leopold LB, Maddock T (1953) The hydraulic geometry of stream channels and some physiographic implications. US Government Printing Office, Washington

Scheidegger AE (1968) Horton's law of stream numbers, Water Resources Res 4(3): 655–658

Shreve RI (1967) Infinite topologically random channel networks, Jour Geol 75: 178–186

Strahler AN (1957) Quantitative analysis of watershed geomorphology, Am Geophys Union Trans 38: 913–920

CHAPTER 3. A HYDROLOGICAL TANK MODEL ASSESSING HISTORICAL RUNOFF VARIATION

3.1. INTRODUCTION

A hydrological cycle describes a water cycle, balance or budget within a drainage basin or on a global scale. Such a cycle can be affected by both natural and anthropogenic factors (Liu and Zheng 2002; Vörösmarty et al. 2000; Wang et al. 2012; Yao et al. 2015; Zhang et al. 2001). As an inductive approach, statistical analyses and a hydrological model are effective tools to assess the impacts of natural and anthropogenic factors on the natural water cycle of the catchment. Among hydrological models, the tank model simply consists of several storage tanks arranged vertically in a series, representing a zonal structure of groundwater in the objective catchment (Sugawara et al. 1995). This study mainly focuses on the rainfall-runoff relation, and the tank model is applied to determine the runoff process that is a part of the hydrological cycle. The objective of this study was to calibrate a tank model in the large catchment lacking meteorological data. We then investigated runoff variation upstream of the Hieu River basin between 1962 and 2014 by applying the calibrated tank model.

3.2. STUDY AREA AND DATA SOURCE

3.2.1. Study area

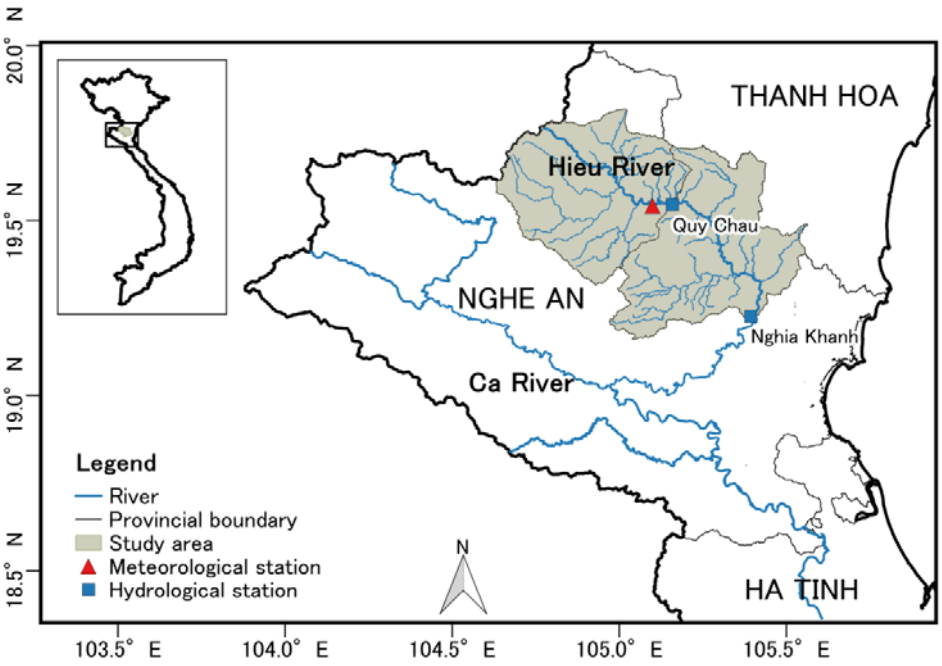

Figure 3.1. Location of the Hieu River Basin

The Hieu River Basin is located at 19°20'N–19°50'N and 104°30'E–105°20'E, and it is the largest tributary on the left bank of the Ca River in Vietnam (Figure 3.1). The catchment area is 5340 km^2 and 228 km long, and it originates from the Pu Hoat Range with an elevation of 2025 m on the Laos-Vietnam border. It flows into the Ca River at Anh Son. The mean slope is 1.3 ppt, and the average riverbed width is 30–35 m; the river network density is 0.71 km/km^2. The river basin is located in the northwest of Nghe An Province, where climatic conditions are characterized by two distinct seasons: the wet season (May to October) and the dry season (November to April). This study investigates the transition of flow regime at the Quy Chau and Nghia Khanh hydrological stations located in the Upper Hieu River. The areas of Quy Chau and Nghia Khanh are 1960 and 4024 km^2, respectively (Chikamori et al. 2012).

3.2.2. Data

Discharge data exist beginning from 1962 at the Quy Chau hydrological station and from 1973 at the Nghia Khanh hydrological station. Meteorological data at Quy Chau include precipitation and evaporation collected over the course of 53 years (1962–2014). All of the data were provided by the North-Central Hydro-meteorological Centre, Vietnam. Evaporation at the station was measured using a Piche tube, but evaporation data are missing for several years. Piche evaporation (E_m) is converted into potential evaporation (E_p) by multiplying by factors of k_1=1.263 and k_2=1.107, where k_1 converts from Piche evaporation to GGI-3000 evaporation according to data from Vinh station from 1961–2000 and k_2 converts from GGI-3000 to actual evaporation of the water surface (Cung, 1979; ENV, 2001).To calculate the actual evaporation of the basin, we assume that evaporation on rainy days was negligible. Therefore, the monthly actual evaporation (E_a) was calculated by multiplying E_p by the ratio of the number of sunny days to the number of total days over a month. However, sunny day data have been available only since 1996. Therefore, the correlations among available meteorological data were investigated to extend the actual evaporation measurements from 1962–2014. The collected data revealed that the average annual precipitation and Piche evaporation at Quy Chau station were 1,668 mm and 732 mm, respectively, over 1962–2014. The highest annual precipitation was 2,482 mm in 1978, and the lowest annual precipitation was 1,102 mm in 1976. The mean annual flow was 77m^3/s between 1962 and 2014 at Quy Chau station and 126 m^3/s between 1973 and 2014 at Nghia Khanh station. The annual discharge at Nghia Khanh was higher than that at Quy Chau by an average of a factor of 1.6. The average monthly flow varied from 15–312 m^3/s at Quy Chau station and from 42–334

m^3/s at Nghia Khanh station. The average monthly discharge of Nghia Khanh was higher than that of Quy Chau, particularly during the flood season.

3.3. METHODS

3.3.1. Rainfall-runoff analysis

3.3.1.1. Tank model

The tank model is a conceptual representation of hydrological processes in the unit area of the basin, and it simulates wetness of several soil layers using tanks arranged vertically in a series. This kind of model typically consists of three or four storage tanks. Precipitation is the input of the model, and it enters into the top tank.

Some of the accumulated water flows through the side outlet of a tank and some of it infiltrates down into the second lower tank. The process repeats for every lower tank. Evapotranspiration is incorporated via subtraction from the tank. The runoff from the side outlet of a storage tank (q) is proportional to the water head over that outlet, and the infiltration (p) is proportional to the water depth. These relations can be expressed as:

$$q = a(h - z), p = bh, \tag{3.1}$$

where h is the tank depth, z is the height of the discharge outlet from the base of each tank, a is the runoff coefficient and b is the infiltration coefficient.

In this study, the tank model with three storage tanks consisted of a surface tank, an intermediate tank, and a base tank (Figure 3.2). The two side outflows from the surface tank are regarded as the surface runoff (q_{11}) and the sub-surface runoff (q_{12}), the side outflow from the intermediate tank is regarded as the intermediate runoff (q_2) and the outflow from the third tank is regarded as the base runoff (q_3). The total outflow from the side outlet (Q) from each tank is regarded as the accumulation of the outflows from a system in the watershed, as given by the following equation:

$$\frac{\mathrm{Q}}{\mathrm{A}} = q_{11} + q_{12} + q_2 + q_3, \tag{3.2}$$

where A is the watershed area.

The tank model introduced by Sugawara for humid regions includes four tanks used to analyze daily discharge from daily precipitation and evaporation inputs (Sugawara et al. 1995). For flood analysis, the tank model includes two tanks, and the inputs are typically precipitation and the outputs are hourly discharge. Many types tank models have been developed for humid regions using daily and hourly data. Nyadawa et al. (1996) proposed a modified tank model that explicitly simulates surface runoff phenomena. These authors verified the model using data from several basins in Kenya. Kuok et al. (2011) ascertained the

best number of tanks in the tank model to provide reliable and accurate estimates of runoff for a rural catchment in a humid region. Mondal et al. (2009) applied the tank model taking into consideration soil-moisture component. Nearly all studies estimating the amount of runoff originating from the catchment area for short-term analysis using daily and hourly input data have made use of a tank model. In this study, we have simulated a tank model for long-term analyses with monthly data. A tank model using monthly data might be associated with less-complex parameters and less difficulty when considering input data for a basin lacking meteorological stations.

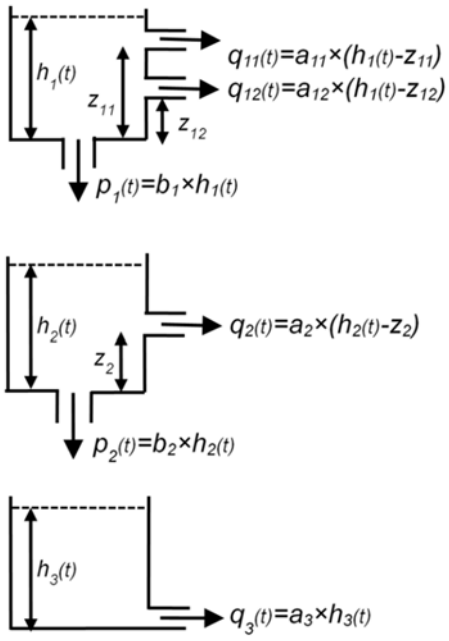

Figure 3.2. Structure of the tank model

3.3.1.2. Calibration of the tank model

We optimized the parameters of the tank model manually using a trial-and-error method. The value of each parameter was successively changed, and the fitness of the simulated hydrograph compared with the observed result was evaluated using the Nash-Sutcliffe efficiency (NSE):

$$\mathrm{NSE} = 1 - \frac{\Sigma(Q_{obs}-Q_{cal})^2}{\Sigma(Q_{obs}-\bar{Q}_{obs})^2}, \tag{3.3}$$

where Q_{obs} represents the observed monthly streamflow, $\bar{Q}_{obs}$ represents the observed monthly mean streamflow and Q_{cal} signifies the calculated monthly streamflow. In addition, the coefficientof determination (R^2) was also used to evaluate the tank model.

To search for the optimal set of parameters, several principles related to the runoff and infiltration coefficients were considered. First, the sum of runoff principles related to the

runoff and infiltration coefficients were considered. The sum of the runoff and infiltration coefficients of a tank has to be less than unity (e.g., $a_{11}+a_{12}+b_1<1$ in the case of the top tank). In other words, the runoff depth from a single tank during a time increment should not exceed the water storage depth of that tank (h) (Sugawara et al. 1995; Basri 2013). Second, the runoff and infiltration coefficients of the lower tank must be smaller than those of the upper tank (i.e., $a_{11}>a_{12}>a_2$). Therefore, the discharge from the lower tank is less than that from the upper tank, which reflects the fact that the discharge from a lower aquifer is typically less than that from an upper aquifer.

3.3.2. Assessment of hydrological regime change

3.3.2.1. Cumulative anomaly

The cumulative anomaly is a statistical method for the visual identification of a variable tendency of discrete data (Wang et al. 2012), and it is used extensively in meteorology. For a discrete series x_i, the cumulative anomaly (X_t) for a data point x_t can be expressed as

$$X_t = \sum_{i=1}^{t}(x_i - x_m),\ t = 1, 2, \ldots, n, \tag{3.4}$$

$$\text{where} \quad x_m = 1/n \sum_{i=1}^{n} x_i; \tag{3.5}$$

x_m denotes the mean value of the series x_i; n represents the number of discrete data points. The cumulative anomaly method can be used to analyze the inflection extent of a discrete data series.

3.3.2.2. Pettitt test

The Pettitt test is a nonparametric method that is widely applied to detect abrupt changes in water discharge (Yao et al. 2015). We employed the Pettitt test using software (R; https://www.r-project.org/). For a given time series X(x_1, x_2,…, x_N) divided into two samples x_1, x_2,…, x_t and x_{t+1}, x_{t+2},…, x_N, the Pettitt test uses a version of the Mann-Whitney statistic $U_{t,N}$ calculated as

$$U_{t,N} = U_{t-1,N} + \sum_{j=1}^{N} \operatorname{sgn}(x_t - x_j), \quad t = 2, 3, \ldots, N, \tag{3.6}$$

where

$$\operatorname{sgn}(x_t - x_j) = \begin{cases} 1, & x_t > x_j \\ 0, & x_t = x_j. \\ -1, & x_t < x_j \end{cases} \tag{3.7}$$

The breakpoint is defined to be where $|U_{t,N}|$ reaches its maximum value:

$$K_N = \operatorname{Max}|U_{t,N}|, \quad (1 \le t \le N). \tag{3.8}$$

The significance level associated with K_N is determined approximately as the following

$$p \cong 2 \exp\left[\frac{-6(K_N)^2}{(N^3+N^2)}\right]. \tag{3.9}$$

If $p < 0.05$, a significant change point exists.

3.4. RESULTS

3.4.1. Evaporation data extension

Before applying the tank model, it is important to calibrate the model, which is viewed as exhibiting superior matching between the calculated and observed runoff. Success in calibrating the tank model depends strongly on data quantity and data quality, challenging aspects in the case of the Upper Hieu River due to the lack of meteorological data. Several years of measured evaporation data are missing: 1962, 1963, 1966, 1967, 1976 and 1977. To infill the missing evaporation data, we investigated the relation between available measured evaporation and precipitation.

Figure 3 shows the relation between average monthly measured evaporation (E_m) and average monthly precipitation (P) over the course of 1962–2014. This figure shows that the ratio of E_m/P and P are negatively correlated. When the precipitation exceeds 50 mm from May through October, the ratio of E_m/P is less than unity. In April and November, the monthly precipitation is approximately 50 mm and the ratio of E_m/P is close to unity. From December through March, the ratio of E_m/P is higher than unity. The strong correlation (R^2=0.97) of E_m/P and P in Figure 3.3 can be used to extract the missing monthly evaporation data from the available monthly precipitation data.

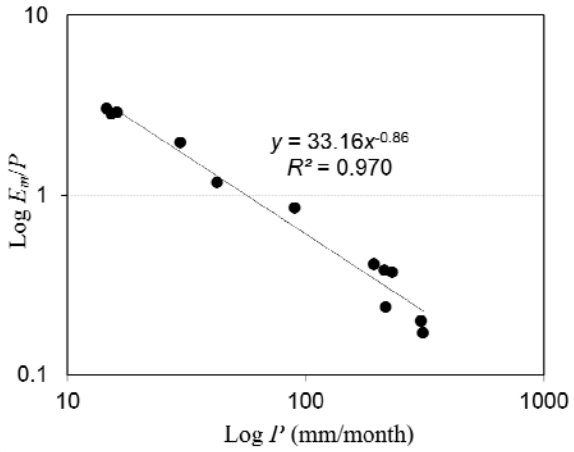

Figure 3.3. Correlation between mean monthly E_m/P and mean monthly P between 1962 and 2014

Monthly actual evaporation E_a was converted from monthly potential evaporation E_p by multiplying E_p by the ratio of the number of sunny days in a month to the total number of days in a month. However, data pertaining to sunny days were only available from 1996–2014. Therefore, the average monthly fraction of sunny days from 1996–2014 was used to extend E_a over 1962–1995. After conducting this extension, we then investigated the correlation

between annual E_a and annual E_p for the entire period of 1962–2014. The strong correlation (R^2=0.94) of E_a and E_p (Figure 3.4) indicated that extended E_a can be used as input data to calibrate the tank model in this study.

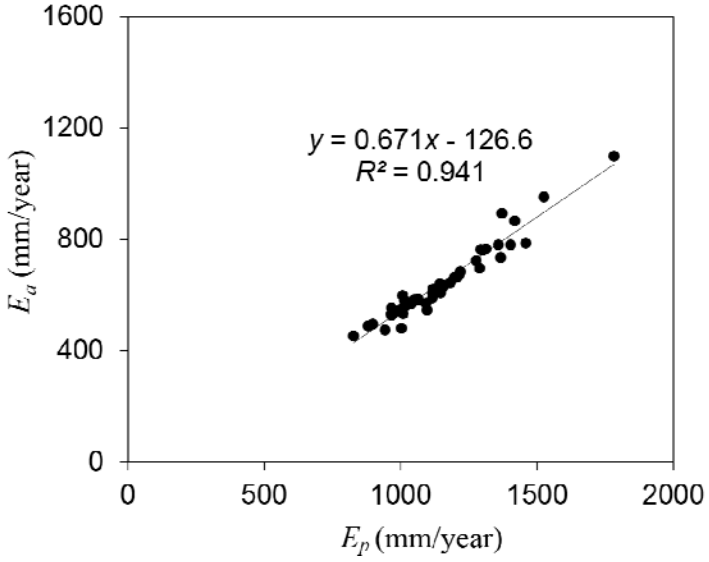

Figure 3.4. Correlation between annual E_p and annual E_a between 1962 and 2014

3.4.2. Change points of annual precipitation and discharge

To determine the turning points of the annual rainfall and discharge from 1962–2014, we used the cumulative anomaly test and the Pettit test. According to the Pettitt test results, there was no change-point year detected at p=0.05. However, change points of annual rainfall series were detected at p=0.48 in 1982. The annual discharge series at Quy Chau station was detected at p=0.21 in 1977. The annual discharge series at Nghia Khanh station was detected at p=0.64 in 1996.

In accordance with the Pettitt test results, the cumulative anomaly test results showed that the turning point of annual rainfall series occurred in 1982 (Figure 3.5a). The turning points of annual discharge series were in 1977 and 1997 at Quy Chau station (Figure 3.5b), and the turning points of annual discharge series were in 1977 and 1996 at Nghia Khanh station (Figure 3.5c).

At the breaking point of 1982, the mean annual rainfall decreased from 1767 mm from 1962–1982 to 1602 mm from 1983–2014 (Figure 3.6a). However, the discharge series increased after 1977 and then subsequently decreased after 1997 at both stations (Figure 3.6b&c).

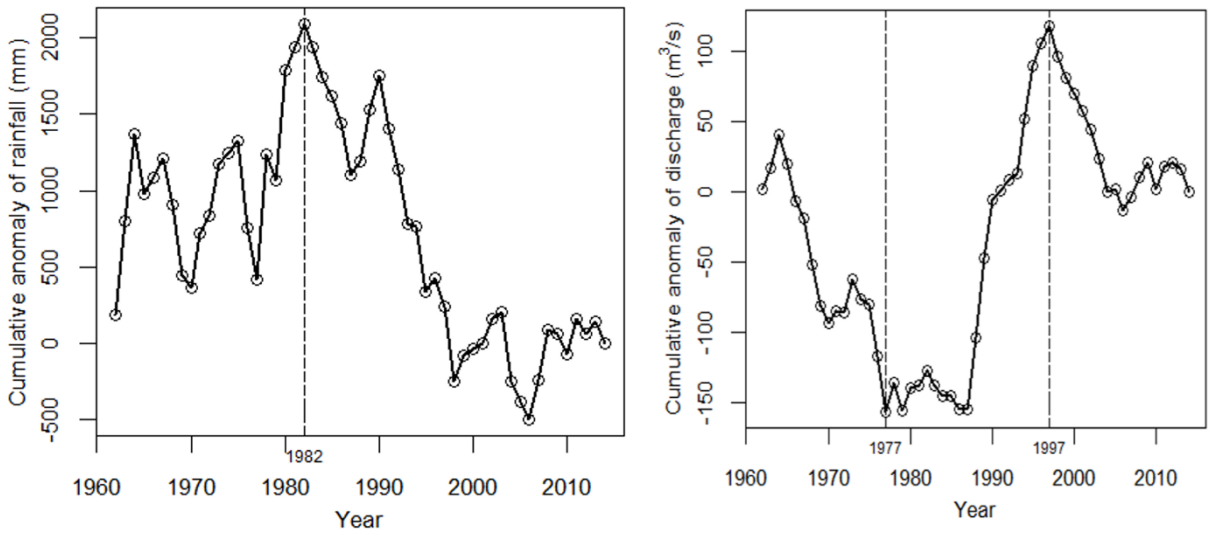

(a)

(b)

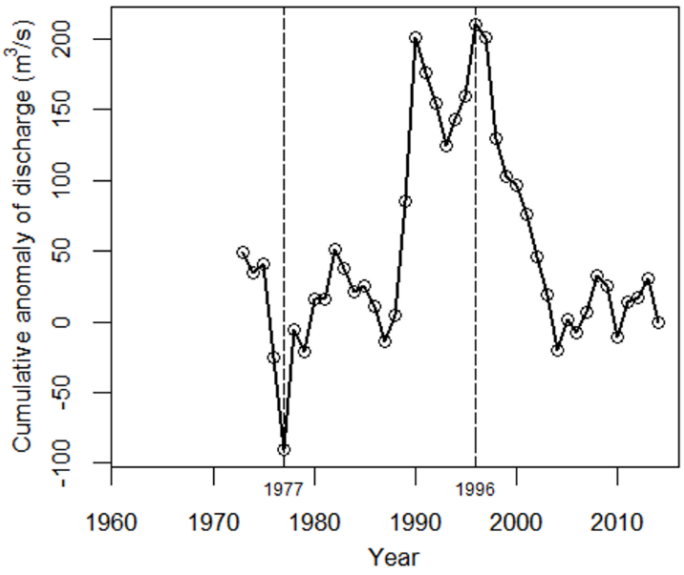

(c)

Figure 3.5. Cumulative anomaly test results of annual rainfall (a), annual discharge at Quy Chau station (b) and annual discharge at Nghia Khanh station (c)

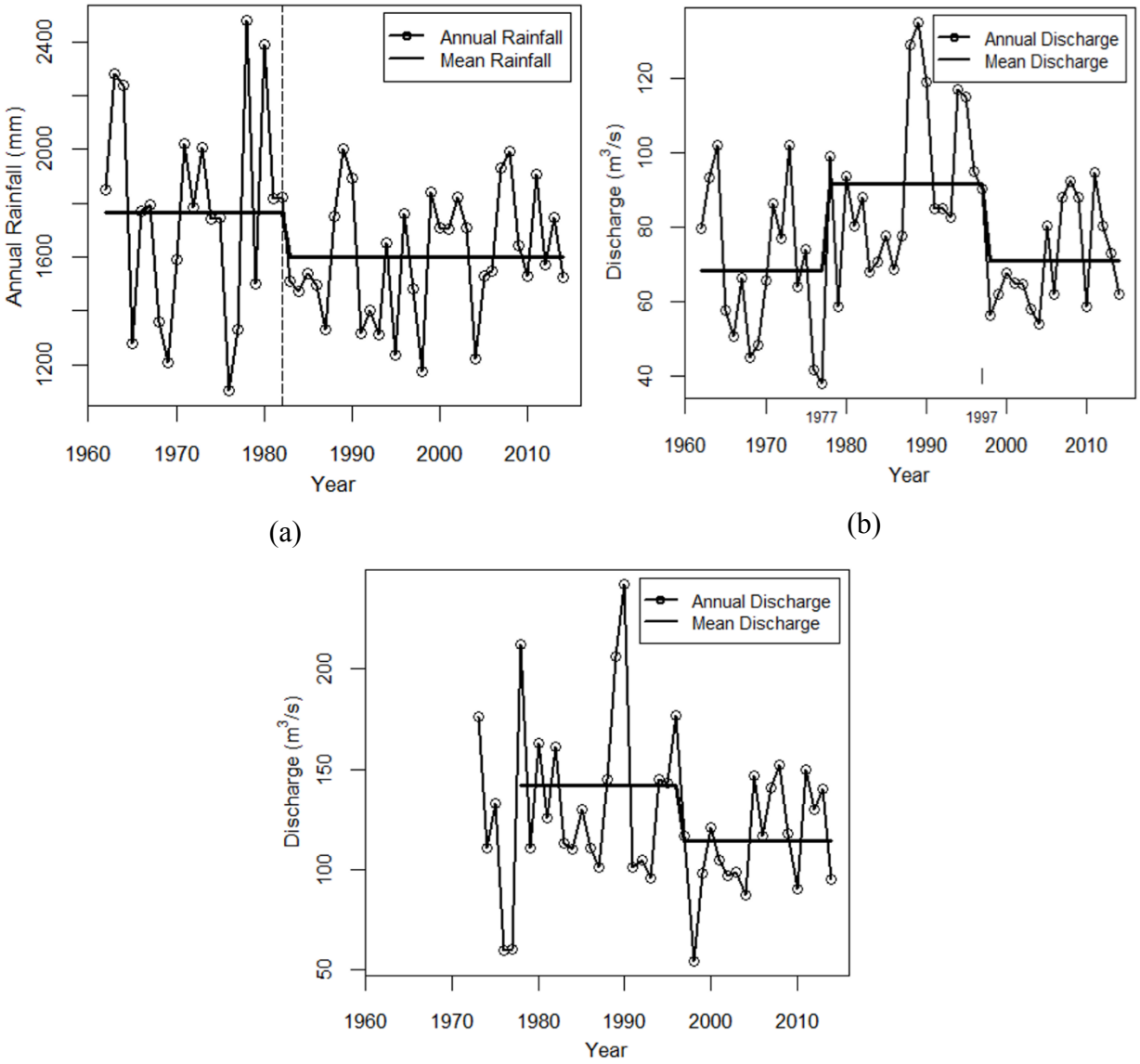

Figure 3.6. Mean annual rainfall (a), mean annual discharge at Quy Chau station (b) and mean annual discharge at Nghia Khanh station (c); break points are identified

3.4.3. Trial of tank model calibration for the whole period of 1962–2014

Prior verification of the annual water balance was conducted for the long-term analyses before calibrating the tank model. In a catchment, the water input and the output must be balanced. However, in the research area, there was only a single meteorological station used for the input data. Therefore, the precipitation might not be representative of the entire catchment. This research assumes that monthly precipitation multiplied by the precipitation factors approximates the annual water balance. In addition, in order to simplify the tank model calibration, the actual evaporation was assumed to be accurate for this study.

Consequently, the annual water balance can be expressed as $P \times C_P = Q + E_a$, where C_P is a precipitation factor (Sugawara et al. 1995).

At the Quy Chau hydrological station, the precipitation factor was 1.13 for 1962–2014. At the Nghia Khanh hydrological station, C_P was close to unity for 1973–2014. We used adjusted precipitation ($P \times C_P$), actual evaporation (E_a) and discharge (Q) to calibrate the tank model.

The calibration results of the tank model show that the base flow of the calculated discharge was consistently smaller than that of the observed discharge for 1984–1998 at both stations (Figure 3.7). Breaking points of the base flow were close to breaking points of precipitation and discharge detected by the cumulative anomaly test and the Pettitt test.

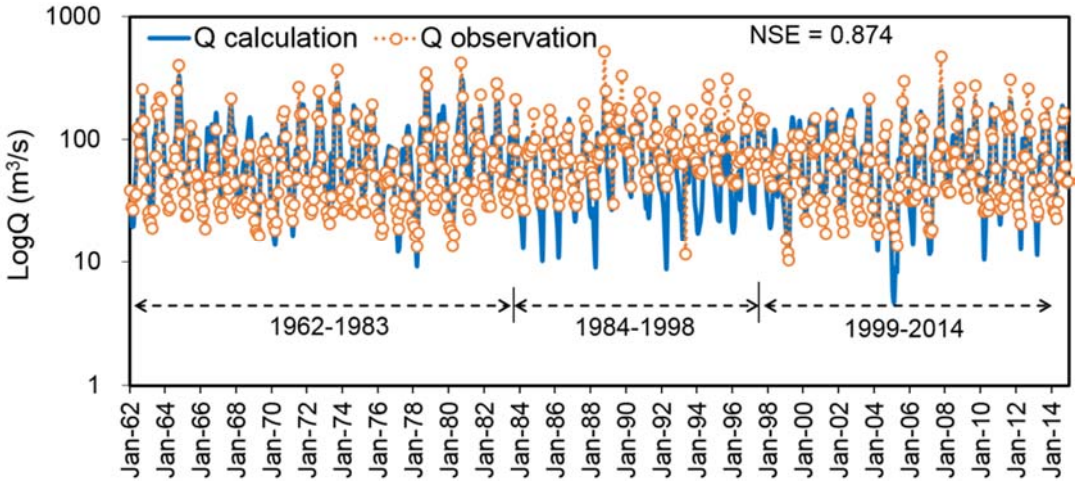

(a)

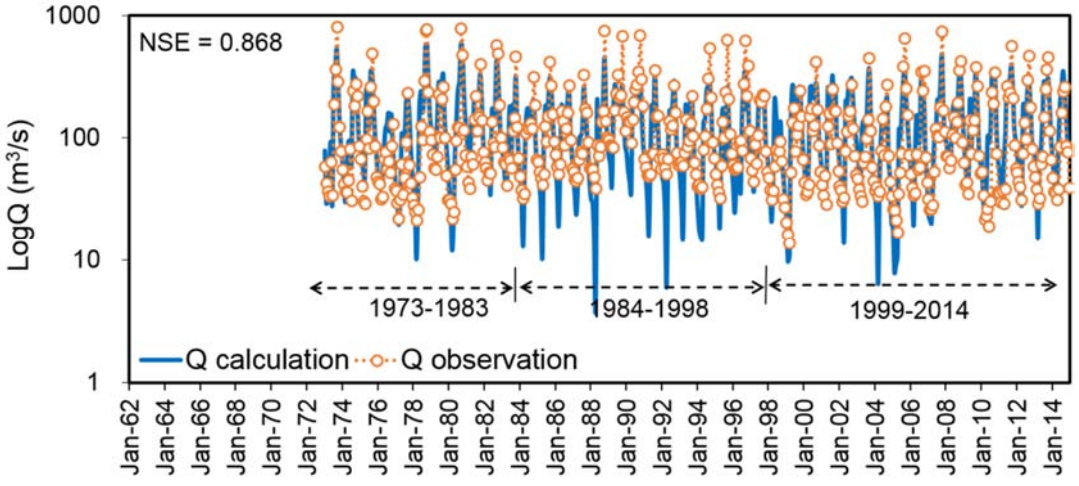

(b)

Figure 3.7. Calibrated tank model (a) at Quy Chau hydrological station for 1962–2014 and (b) at Nghia Khanh hydrological station for 1973–2014

3.4.4. Tank model calibration for the first period (1962–1983) at Quy Chau station

The study was divided into three time periods for additional study: pre-1984 (period 1), 1984–1998 (period 2) and post-1998 (period 3). We first simulated the tank model for period 1 and then applied the simulated parameters for periods 2 and 3. The value of the precipitation factor during each period was estimated using the annual water balance equation of $P_i \times C_{Pi} = Q_i + E_{ai}$, where C_{Pi} is a precipitation factor during each period and i = 1, 2, 3 denotes the first, second and third periods, respectively. At Quy Chau, the results of C_{Pi} were 1.01 for the first period, 1.38 for the second period and 1.10 for the third period. At Nghia Khanh, the corresponding C_{Pi} values were 0.92, 1.08 and 0.96, respectively. The relative change in precipitation was calculated as $(C_{Pi}–1)\times100\%$. We found a significant lack of precipitation, with 38% at Quy Chau and 8% at Nghia Khanh during period 2.

The rainfall data at Quy Chau station were appropriate for catchment representation for periods 1 and 3, however insufficient to meet the water budget for period 2. Adjusting the precipitation by multiplying by a precipitation factor is apparently a simple method used for long-term analyses. However, the precipitation factor also shows a seasonal change (Sugawara et al., 1995). Therefore, using a precipitation factor that varies by month might yield better calibration results. In this case, the precipitation factor is described as $C_P(M)$, where M is the month index (Sugawara et al. 1995). In this study, $C_P(M)$ was calibrated by the number of trials.

The tank model was calibrated for period 1 (1962–1983) corresponding to two trials.

(1) Trial No. 1: Precipitation adjusted by multiplying by a constant precipitation factor. However, C_P at Quy Chau during 1962–1983 was close to 1.0. Therefore, the precipitation did not change.

(2) Trial No. 2: Precipitation was adjusted by precipitation factor $C_P(M)$ (Sugawara *et al.*, 1995). The available precipitation data were adjusted taking into consideration a high peak discharge. After the trials, the appropriate values of $C_P(M)$ were changed corresponding to different range of discharge. When the monthly discharge exceeded 400 m^3/s, the precipitation was multiplied by $C_P(M)$=1.5. If the monthly discharge was between 200 and 400 m^3/s, the precipitation was multiplied by $C_P(M)$=1.2. If the monthly discharge was less than 38 m^3/s, the precipitation was not changed. The precipitation factor for the other months was 1.0.

In Figure 3.8, we show the results of tank model calibration for the two trials at Quy Chau station. The NSE and the coefficientof determination (R^2) of trial No. 1 are 0.947 and 0.846, respectively. The coefficients of trial No. 2 are 0.964 and 0.884, respectively. Figure

3.9 shows the improvement in trial No. 2 (b) compared with trial No. 1 (a) based on the better fit of the duration curve.

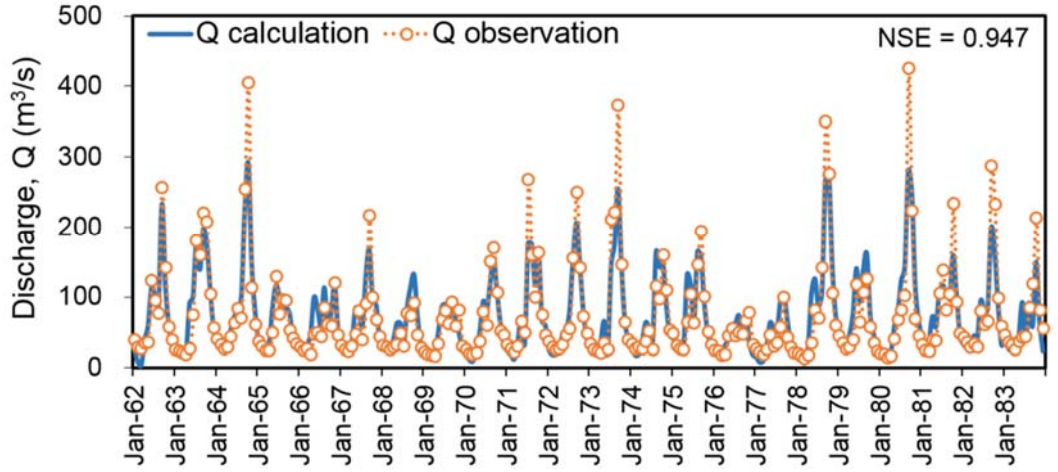

(a)

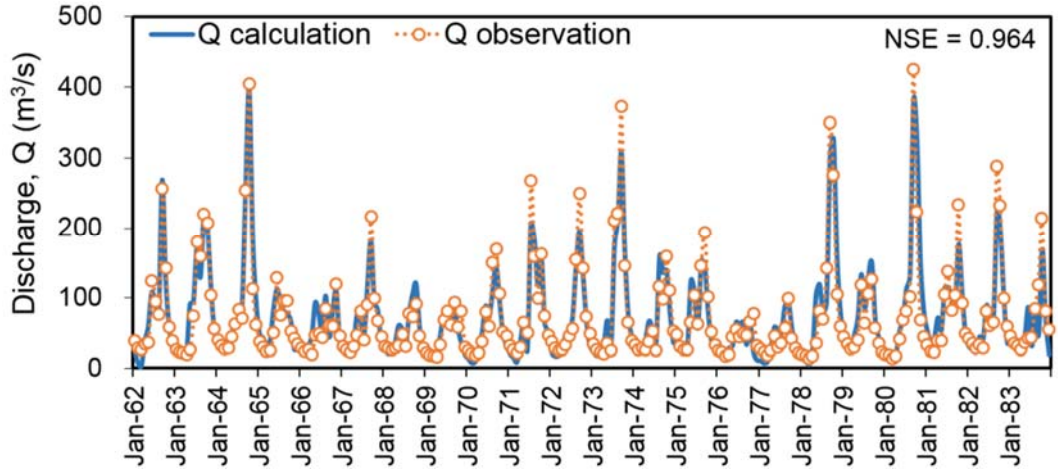

(b)

Figure 3.8. Calibrated tank model at the Quy Chau gauging station from 1962–1983 trial No. 1 and (b) trial No. 2

3.4.5. Tank model calibration for the first period (1973–1983) at Nghia Khanh station

The tank model calibrated for 1973–1983 at Nghia Khanh made use of the same method as that applied to Quy Chau station. The appropriate values of $C_P(M)$ must be changed to correspond to a different range of monthly discharges. When the monthly discharge exceeds 400 m^3/s, the precipitation is modified by multiplying it by $C_P(M)$=1.4. If the monthly discharge is less than 64 m^3/s, the precipitation was left unchanged. The precipitation factor for the remaining months was 0.92.

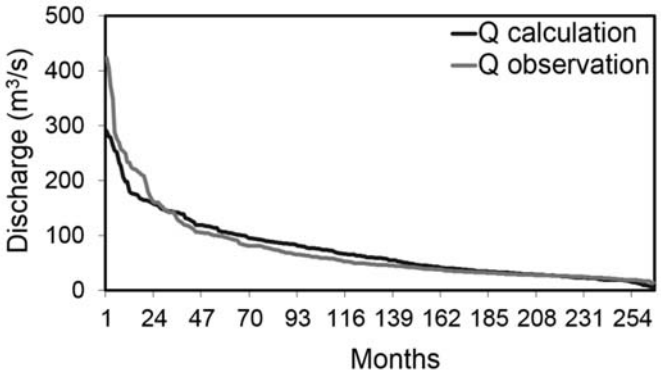

(a)

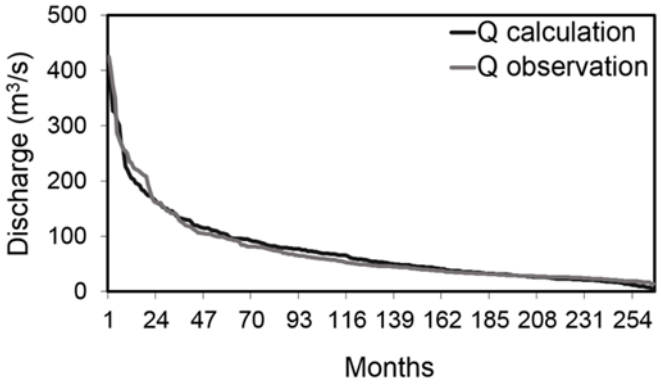

(b)

Figure 3.9. Duration curves at Quy Chau station from 1962–1983
(a) trial No. 1 and (b) trial No. 2

The results of the tank model calibration of the two trials at Nghia Khanh station are shown in Figure 3.10. The NSE and R^2 values of trial No. 1 were 0.894 and 0.821, respectively. The corresponding values for trial No. 2 were 0.937 and 0.905, respectively. An improvement in calibration was noted for trial No. 2 compared with trial No. 1 (Figure 3.11). These results indicate that a precipitation factor that varies with the month is useful for obtaining better calibration results. A month that has higher precipitation (discharge) necessitates a higher precipitation factor, which means that rainfall density might lead to a change in the relation between rainfall and infiltration, as well as surface runoff in the watershed (Basri 2013).

3.4.6. Tank model validation

The calibrated parameters in Figure 3.12 were applied to periods 2 and 3. A similar $C_P(M)$ was applied for periods 2 and 3 as for period 1 (trial No. 2). The model evaluation statistics for different periods are listed in Table 3.1. Our results indicate that the tank model applied for period 3 had better results of the NSE and R^2 values than for period 2 at both stations. A significant effect was noted for the natural hydrological cycle of the basin during

period 2. The results of the NSE and R^2 values for periods 2 and 3 in this study were in line with the findings of Giang et al. (2014) (Table 3.1). These authors applied the SWAT model to the Upper Ca River. They found that, compared with the calibration period (1971–1995), the simulated discharge during the validation period (1996–2010) more closely followed the corresponding observed discharge; it underestimated the peak-flow months less and overestimated the low-flow months less.

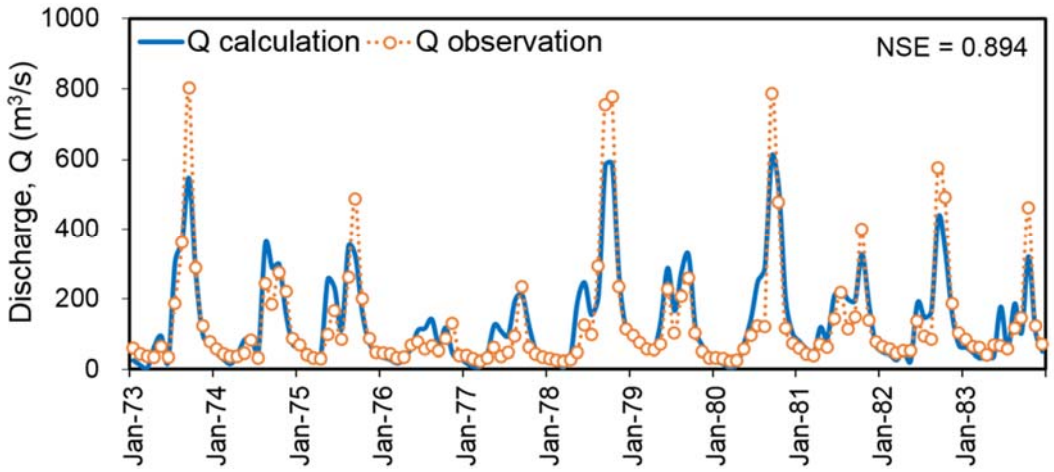

(a)

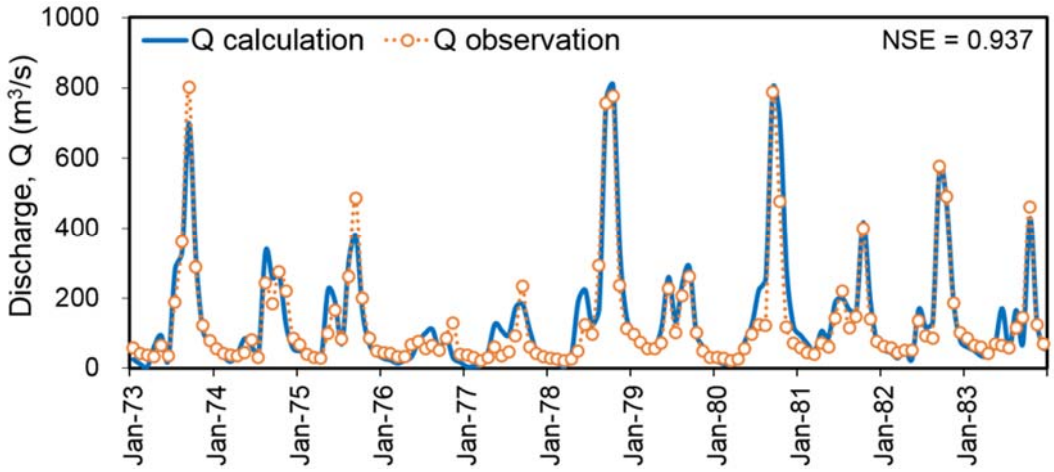

(b)

Figure 3.10. Calibrated tank model at Nghia Khanh station from 1973–1983 (a) trial No. 1 and (b) trial No. 2

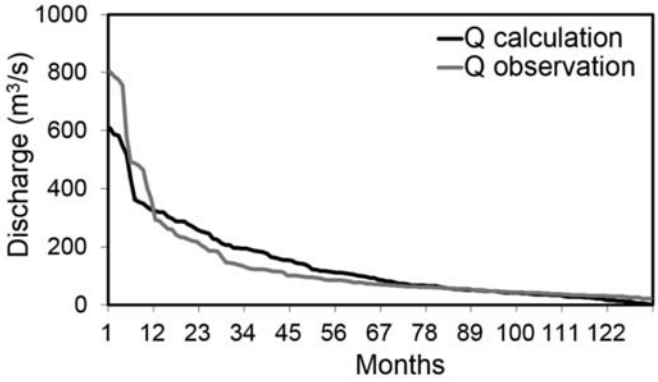

(a)

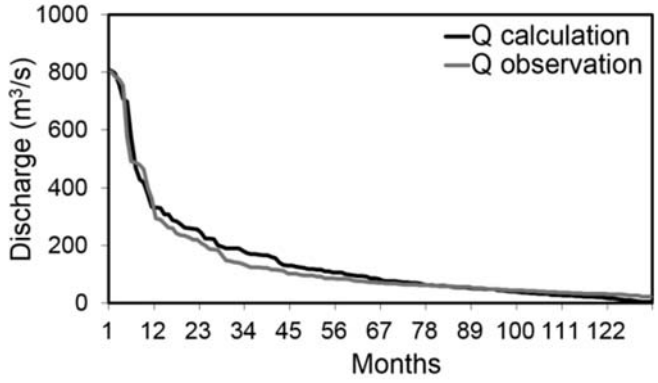

(b)

Figure 3.11. Duration curves at Nghia Khanh station from 1973–1983 (a) trial No. 1 and (b) trial No. 2

Table 3.1. Nash-Sutcliffe efficiency (NSE) and the coefficient of determination (R^2) resultsfor different time periods

Stations	Quy Chau (1960 km^2)		Nghia Khanh (4024 km^2)		Yen Thuong (23,000 km^2) (Giang et al. 2014)	
Periods	1984–1998	1999–2014	1984–1998	1999–2014	1971–1995	1996–2010
NSE	0.895	0.920	0.892	0.896	0.86	0.89
R^2	0.665	0.830	0.762	0.815	0.87	0.89

3.5. DISCUSSION

3.5.1. Tank model calibration using monthly input data

The tank model was calibrated for period 1 at the Upper Hieu River using the three-tank structure (Figure 3.2). However, the side outlet and infiltration coefficients for the third tank had very little effect on the simulation results. Therefore, the tank model composed of two tanks using monthly data was the most appropriate for simulating the Upper Hieu River Basin. The set of simulated parameters of trial No. 2 at each station is shown in Figure 3.12.

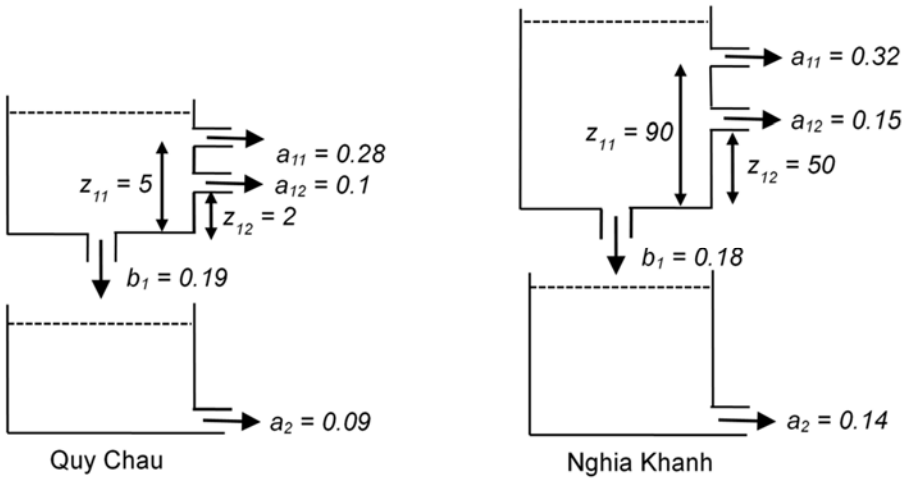

s

Figure 3.12. Calibrated parameters of the tank model using monthly data

Previous researchers have investigated the most appropriate number of tanks for the tank model. For example, Kuok et al. (2011) investigated three-tank, four-tank and five-tank models to ascertain the most appropriate tank model configuration for the southern region of Sarawak in Malaysia. These authors revealed that the four-tank model yielded the best runoff forecasting result. Kadarisman(1993) applied the tank model for the Babak River Basin, Lombok Island, Indonesia and concluded that the tank model with three tank components was unsuitable for use in low-flow analysis. The tank model with three tank components can be used for normal and high-accuracy analysis in cases in which the low flows are not significant. Basri (2013) used the tank model with various types of land as a reference to determine the preferred number of tanks. This author advised using tank models of different types based on land use (e.g., four tanks for a forest, three tanks for a garden or vacant lot, two tanks for a paddy and one tank for a settlement). The number of tanks therefore depends on the catchment area. Pradhan (2001) reported that the numbers of tanks necessary for the tank model increases for larger-scale catchments to ensure better performance of the model. In nearly all earlier studies, daily data were used to calibrate the tank model (Kuok et al. 2011; Mondal et al.2009; Pradhan 2001). In this study, monthly data were used as the input for the tank model. We found that a two-tank model with monthly input data was the most appropriate tank model for the Upper Hieu River.

3.5.2. Temporal change of runoff at the Upper Hieu River

The temporal change in runoff upstream of the Hieu River Basin was investigated for three time periods: prior to 1984, 1984–1998 and after 1998. Figures 3.13 shows the results of double mass curves of precipitation-calculated discharge and precipitation-observed discharge. These data indicate that the increment of observed discharge was less than the increment of calculated discharge during period 3. The annual loss in discharge was 0.2×109 m3 at Quy

Chau and 1.5×109 m3 at Nghia Khanh between 1999 and 2014. This finding means the rate of discharge loss in the Lower Basin (between Quy Chau and Nghia Khanh) was approximately six times higher than that in the Upper Basin (upstream of Quy Chau).

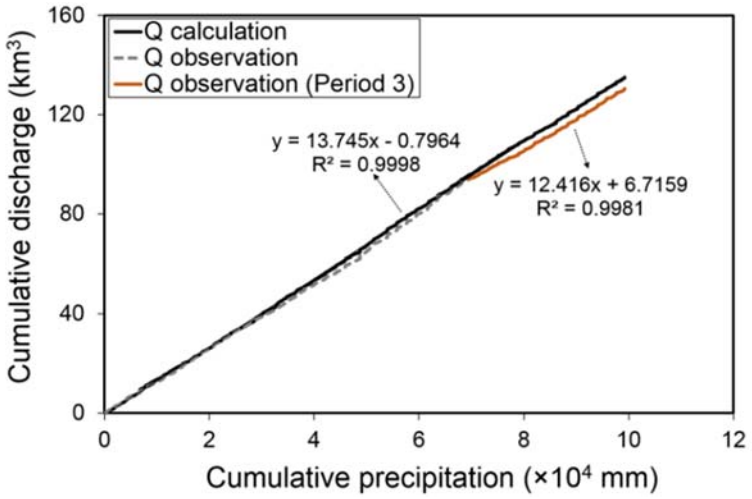

(a)

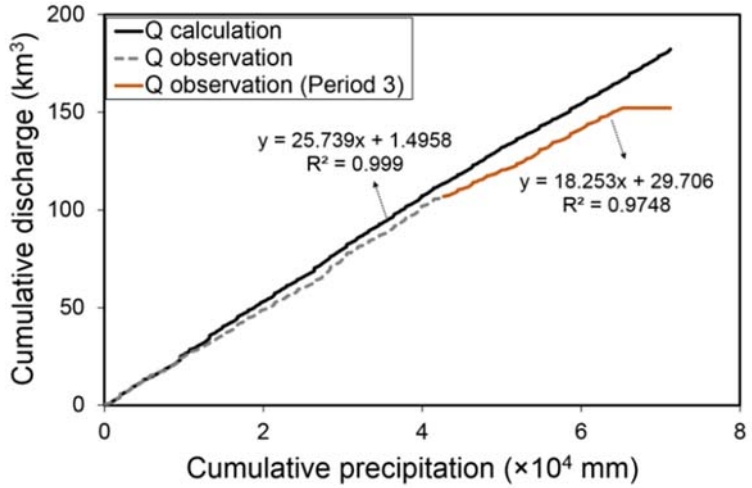

(b)

Figure 3.13. Double mass curves of precipitation and discharge
(a) Quy Chau and (b) Nghia Khanh

It has been reported that the annual runoff of many rivers around the world has decreased remarkably during recent decades (Shiklomanov 1993). The decrease in precipitation and/or the increase in evapotranspiration are considered to be factors that directly influence runoff decrease (Wang et al. 2012). The decrease in runoff might also result from anthropogenic influences in the catchment (e.g. population growth, river regulation, dam construction, irrigation) (Vörösmarty et al.2000; Yao et al. 2015). At the research site, the actual evaporation that we found also exhibited an increasing trend for the last 53 years, which resulted in reduction in runoff. In addition, many reservoirs have been constructed and

operated at upper Quy Chau since 2005 (e.g., Ban Kok, Sao Va and Nhan Hac, which have electricity generation capacities of 18, 3, and 45 MW, respectively). There are two major reservoirs between Quy Chau and Nghia Khanh: Sao-River reservoir and Ban Mong reservoir. Construction of the Sao River reservoir, with a gross capacity of 5.1×10^7 m^3, started at the end of 1999 and finished in 2003. It was designed to provide irrigation water for 6200 ha of land for rice cultivation, commercial crops and water reserves. Ban Mong reservoir, with a gross capacity of 2.5×10^8 m^3 and a power generation capacity of 42 MW, was first started in 2010 and ultimately completed in 2012. The reservoirs provide power generation, and water supply for residential and farming areas in the region. Moreover, they reduce flooding of the Hieu River downstream. All of the water used for agricultural and residential purposes, in addition to the water stored in the reservoirs, resulted in a marked decrease in the river runoff in the Hieu River Basin beginning in 1998, particularly at Nghia Khanh. In addition, the reservoir might engender increased potential evaporation and leakage losses, resulting in decreased runoff (Gao et al. 2011).

3.6. CONCLUSIONS

We have used a tank model calibrated with monthly input data to assess the temporal variation in river flow at the Upper Hieu River Basin in Vietnam during the time period 1962–2014. With cumulative anomaly tests and Pettitt tests, we detected turning points in annual rainfall and discharge. Our results reveal turning points in annual rainfall series in 1982 and turning points in the annual discharge series in 1977 and 1997 at Quy Chau. At Nghia Khanh, we noted turning points in the annual discharge series in 1977 and 1996. In addition, we calibrated the tank model at both stations for the 53 years of observations. The base flow of the calculated discharge was less than that of the observed result from 1984–1998. We assessed the flow variation for three time periods: 1962–1983 (period 1), 1984–1998 (period 2) and 1999–2014 (period 3).

The value of the precipitation factor during each period was estimated by checking the annual water balance. The tank model was simulated for period 1. Then, we applied the calibrated parameters to periods 2 and 3. The precipitation and evaporation used as input data for calibrating the tank model came from a single meteorological station model with a catchment area of 1960 km^2 at Quy Chau and 4024 km^2 at Nghia Khanh. The results of tank model calibration indicated that the hydrographs improved when we used a precipitation factor as a function of the month. In addition, our results confirmed that a two-tank model with monthly input data is the most appropriate tank model for the Upper Hieu River. We

used the set of calibrated parameters applied to periods 2 and 3 to ascertain the temporal variation in the flow on the Upper Hieu River. The temporal variation of river flow was investigated by comparing the increase in calculated and observed discharges with increases in precipitation. A marked decrease in runoff has occurred since 1999, particularly at Nghia Khanh station. The rate of discharge loss in the Lower Basin was approximately six times higher than that in the Upper Basin, a finding likely due to reservoir construction and water being intensively used for agricultural and residential purpose.

REFERENCES

Basri H (2013) Development of rainfall-runoff model using tank model: Problems and challenges in province of Aceh, Indonesia. Aceh Int J Sci Technol 2(1): 26–36

Chikamori H, Heng L, Daniel T (eds) (2012) Catalogue of rivers for Southeast Asia and the Pacific – Volume VI. UNESCO-IHP Regional Steering Committee for Southeast Asia and the Pacific

Cung NV (ed) (1979*)* Technical Manual for Irrigation. The Agricultural Publishing House, Ha Noi. (In Vietnamese)

ENV–Vietnam Electricity (2001) Feasibility study for Ban La hydropower project, meteorological condition. Ha Noi, Vietnam. (In Vietnamese)

Gao P, Mu X-M, Wang F, Li R (2011) Changes in streamflow and sediment discharge and the response to human activities in the middle reaches of the Yellow River. Hydrol Earth Syst Sci 15: 1–10

Giang PQ, Toshiki K, Sakata M, Kunikane S, Vinh TQ (2014) Modelling climate change impacts on the seasonality of water resources in the upper Ca river watershed in Southeast Asia. Sci World J

Kadarisman (1993) A comparative study of the application of two catchment models to the Babak River Basin Lombok Island – Indonesia. Memorial University of Newfoundland. Retrieved from http://research.library.mun.ca/id/eprint/5308

Kuok K, Harun S, Chiu P-C (2011) Investigation best number of tanks for hydrological tank model for rural catchment in humid region. J Inst Eng, Malays 72(4): 1–11

Liu C, Zheng H (2002) Hydrological cycle changes in China`s large river basin: The Yellow River drained dry. In M. Beniston (ed), Climatic Change: Implications for the Hydrological Cycle and for Water Management (pp. 209–224). Kluwer, Dordrecht

Mondal MS, Kouchi Y, Okubo K (2009) Sedimentation and thermal stratification during floods: A case study on Hail Haor of North-East Bangladesh. J Hydrol Meteorol 6(1): 15–25

Nyadawa MO, Kobatake S, Ezaki K (1996) A modified tank model and applications in some river basins in Kenya. Jpn Soc Hydrol Water Res 9(6): 498–512. Retrieved from https://www.jstage.jst.go.jp/article/jjshwr1988/9/6/9_6_498/_article

Pradhan NR (2001) Applicability of BTOPMC model and tank model in sub-catchments of Sun Kosi Basin, Nepal. Tribhuvan University

Shiklomanov I (1993) World fresh water resources. In P. H. Gleick (ed), Water in crisis a guide to the world's fresh water resources (pp. 13–24). Oxford University Press, New York

Sugawara M (1995) Chapter 6: Tank model. In V. P. Singh (ed), Computer models of watershed hydrology (pp. 165–214). Water Resources Publications, Highlands Ranch, Colorado

Vörösmarty CJ, Green P, Salisbury J, Lammers RB (2000) Global water resources: vulnerability from climate change and population growth. Science 289(5477): 284–288

Wang S, Yan M, Yan Y, Shi C, He L (2012) Contributions of climate change and human activities to the changes in runoff increment in different sections of the Yellow River. Quat Int 282: 66–77

Yao H, Shi C, Shao W, Bai J, Yang H (2015) Impacts of climate change and human activities on runoff and sediment load of the Xiliugou Basin in the Upper Yellow River. Adv Meteorol

Zhang L, Dawes WR, Walker GR (2001) Response of mean annual evapotranspiration to vegetation changes at catchment scale. Water Res 37(3): 701–708

CHAPTER 4. EFFECTS OF DAM CONSTRUCTION ON TOTAL SOLIDS

4.1. INTRODUCTION

The total solid load is controlled by Earth system drivers (e.g., climate, basin relief, basin geology, and drainage basin area) (Brinkmann 1989; Meybeck 2003; Milliman and Farnsworth 2011). It has been reported that rivers discharge more than 19 billion tons of solids and 3.8 billion tons of dissolved matters annually into the global ocean (Milliman and Farnsworth 2011). The correlation between particulate and dissolved matters yields demonstrates the dependence of chemical weathering on the extent of physical weathering, which reflects the natural background of particular rivers. This linkage enables approximate hydrogeochemical classification. For example, Brinkmann (1989) classified river water as whitewater, clearwater, blackwater, and mixed waters based on the range and relationship between total dissolved solids and total suspended solids. Milliman and Farnsworth (2011) classified river systems as dissolved-dominated and sediment-dominated according to the total suspended solids-to-total dissolved solids (TSS-to-TDS) ratio. These authors reported that dissolved-dominated rivers are particularly prevalent in Europe and Eurasia.

Anthropogenic activities (e.g., river damming) have drastically modified the flux of natural river material (Meybeck 2003). A persistent change in water discharge and sediment load because of dam regulation can result in disequilibrium between supplied sediment and released sediment (Andrews 1986). Consequently, dams can alter natural river regimes (Chien 1985) and modify a river's morphology and riverbed characteristics (Meybeck 2003). A reservoir can regulate river flows by, for example, suppressing floods, raising the base flow, and catching coarse sediments and passing finer silt only (Eiriksdottir et al. 2017; Xu 2007; Yang et al. 2017). When eutrophication occurs in a reservoir, nutrient and silicate deficiencies can be observed downstream of the dam. This situation can cause a change in ion constitution and affect biogeochemical cycling in coastal seas (Friedl and Wüest 2002; Humborg et al. 1997).

Located in Southeast Asia, Vietnam possesses one of the largest dam networks in the world. This network comprises more than 7000 dams of different types and sizes (Amos et al. 2017). The Ca River is one of the largest basins in Vietnam, and it currently included numerous dams built for power generation, flood control, and water supply. This study aims to assess the impact of dam construction in the upper Ca River by evaluating the suspended sediment load in a downstream hydrological station. Additionally, this study discusses the suspended sediment transport in the Ca River in north-central Vietnam and compares results

with theoretical methods. The research period was divided into a pre-dam period (1994–2004) and a post-dam period (2005–2014) for quantitative comparison. The dissolved solid load is not available for long-term periods, but it is available by applying the loading L_{DS}–Q curves for dissolved solids obtained from field measurements.

4.2. STUDY AREA AND DATA

The study was performed in the Ca River basin, which is the third largest river in north-central Vietnam, located between 18°15′00″N and 20°10′30″N and 103°45′20″E and 105°15′20″E (Figure 1). The main flow of the river originates from Mt. Muong Khut and Mt. Muong Lap (1,800–2,000 m) in Lao People's Democratic Republic (PDR). It runs in a northwest-southeast direction, crossing Lao PDR's Xiangkhouang Province and Vietnam's Nghe An and Ha Tinh provinces, and it flows out into the East Sea through Cua Hoi. The total basin area is 27,200 km^2, including 17,730 km^2 in Vietnam's territory. The main river length is 531 km, of which 170 km runs through Lao PDR and 361 km runs through Vietnam. The river network density is 0.6 km/km^2. The topography of the Ca River is very diverse with a general slope in the West-East, Northwest-Southeast, Southwest-Northeast. The mountainous terrain accounts for 60% to 70% of the catchment area, which is mainly a watershed protection forest. Midland hills have a height of 20 m to 200 m, accounting for about 25% to 35% of the area. The Ca River plain is located along both sides of the river, small and narrow, with the elevation gradually changing from 15 m to 0 m, accounting for about 10% of the basin area. In terms of geological characteristics, the area of Ca river fault zone distributes geological formations with early and middle Paleozoic age to Quaternary age. Sedimentary formations occupy most of the area. Soil types are formed from the parent rocks which are concentrated mainly in hilly and mountainous areas; Ferralsol in particular (accounting for 83.51%) (IWRP 2012). Except for the alluvial soils in the low valleys, soils in the area are generally acidic, poor in nutrients, and highly susceptible to erosion (Giang et al. 2007).

Many reservoirs have been built in the Ca River basin: the reservoirs of Ban Ve and Khe Bo on the main stream of the Ca River, the Ban Mong reservoir on the Hieu River, and the Sao River reservoir located in a tributary of the Hieu River. These multi-purpose reservoirs are used for hydropower generation, water supply, irrigation, and flood and drought control. The Ban Ve reservoir is the largest hydropower project on the Ca River and also the largest hydropower project in north-central Vietnam. It has a capacity of 320 MW, and construction began at the end of 2005. Additionally, many other reservoirs have been built on small rivers and streams of the Ca River. These reservoirs have a small capacity and are used mainly for irrigation purposes.

In this study, data were collected at the Dua (105°02′20″E and 18°59′20″N) and Yen Thuong hydrological stations (105°23′00″E and 18°41′10″N) during the time period 1994–2014. Both stations are located in the downstream of the Ca River with an elevation of 16 m at Dua station and 4 m at Yen Thuong station. The yearly flow regime is divided into two distinct seasons: flood season (from June to November) and dry season (from December to May). The respective basin areas at Dua and Yen Thuong are 20,800 and 23,000 km^2 (Chikamori et al. 2012). The collected data include daily discharge, hydrological regime, and suspended sediment concentration. The dissolved solids data were not available at both the stations, but electrical conductivity (EC) data at the Dua station were available for several years beginning in 2000. All of the data were provided by the North-Central Hydro-meteorological Centre of Vietnam. The collected data revealed that the mean annual flow ranges between 221 and 902 m^3/s with an average 571 m^3/s at Yen Thuong in 1994–2014. The mean annual flow ranges between 109 and 635 m^3/s with an average 407 m^3/s at Dua.

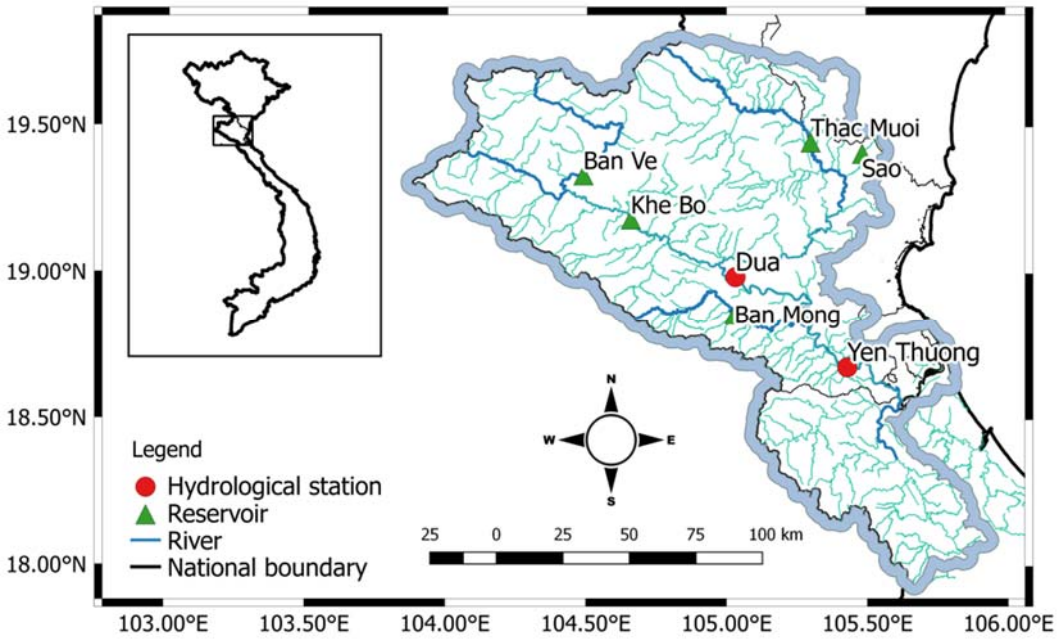

Figure 4.1. Map of the Ca River

4.3. METHODS

4.3.1. Station hydraulic geometry

The relationship between a river's discharge and hydraulic variables such as its width, depth, and velocity in river cross sections are expressed as power functions, which are also described by the term "at-a-station hydraulic geometry" (Leopold and Maddock1953):

$$b = b_1\hat{Q}^{b_0},\ \ h = h_1\hat{Q}^{h_0},\ \ \bar{u} = u_1\hat{Q}^{u_0},\ \ b_1h_1u_1 = 1,\ \ b_0 + h_0 + u_0 = 1, \tag{4.1}$$

where$b$, h, and $\bar{u}$ are the width, depth, and average velocity, respectively, of the river's cross section. The normalized discharge is $\hat{Q} = Q/Q_1 = \bar{u}bh/u_1 b_1 h_1$ and b_1, h_1, and u_1 represent the dimensional intercepts of the regime curves at $Q = Q_1$, the unit discharge. The values b_0, h_0, and u_0 are the power exponents of discharge related to the width, depth, and average velocity, and they also represent the slope of the regime laws.

4.3.2. Calculation of suspended sediment load

In this study, suspended sediment load was estimated using a hydrological approach. We adopted the hydraulic geometry of Leopold and Maddock (1953) by making a dimensional consideration and using the concentration formula given by Celik and Rodi (1991) and an average velocity of the river's cross section. As a result, the suspended sediment load formula only depends on Manning's roughness coefficient and particle size. The calculation of suspended sediment load is as follows.

Suspended-sediment discharge is estimated by Eq.(2):

$$L_{ss} = \bar{c}\rho_s \bar{u}bh, \tag{4.2}$$

where L_{ss} [kg/s] is the sediment discharge, Q [m^3/s] is water discharge, ρ_s = 2,650 [kg/m^3] is the sediment density, $\bar{c}$ is the average volumetric concentration of suspended sediment, $\bar{u}$ [m/s] is the flow velocity, h [m] is the depth, and b [m] is the width of the channel.

The bulk sediment concentration can be replaced by that of the maximum possible transport $\bar{c}$, with which no sedimentation occurs along the river, as given by Celik and Rodi (1991):

$$\bar{c} = 0.034 \frac{u_*^2 \bar{u}}{\sigma g h w_s}, \tag{4.3}$$

where u_* is the friction velocity [m/s] that is assumed to be a constant, $\sigma = 1.65$ is the submerged specific weight, w_s is the settling velocity [m/s], and g = 9.8 [m/s^2] is the gravitational acceleration.

The friction velocity and the Manning equation are given by:

$$u_* = \sqrt{gRI_e} \tag{4.4}$$

$$n = \bar{u}^{-1} R^{2/3} I_e^{1/2}, \tag{4.5}$$

where R is the hydraulic radius, I_e is the energy grade, and n is Manning's roughness coefficient. Replacing R by h and adapting Eqs.(4.3)–(4.5) to Eq.(4.2), the suspended-sediment discharge can be re-written as follows:

$$L_{ss} = 0.034 \frac{\rho_s n^2}{\sigma w_s} \bar{u}^4 b h^{-1/3} = \frac{54.6 n^2}{w_s} \bar{u}^4 b h^{-1/3} \tag{4.6}$$

The regime law, Eq.(4.1), is used in the equations above to obtain the suspended sediment discharge as follows:

$$L_{ss} = \frac{54.6 n^2}{w_s} \bar{u}_1^4 b_1 h_1^{-1/3} Q^{4u_0 + b_0 - h_0/3} \tag{4.7}$$

We used Eq.(4.7) to estimate suspended sediment load. As shown in the equation, sediment load depends on Manning's roughness coefficient, settling velocity, and major hydraulic characteristics.

The settling velocity is estimated based on the suspended non-cohesive particle size (Habini 1994):

$$w_s = \begin{cases} \sigma g D^2 / 18\nu \ for \ D \le 0.1 \ mm \\ (10\nu / D)\left\{\left[1 + (0.01\sigma g D^3 / \nu^2)\right]^{0.5} - 1\right\} \ for \ 0.1 \ mm < D < 1.0 \ mm \\ 1.1(\sigma g D)^{0.5} \ for \ 1.0 \ mm \le D \end{cases} \tag{4.8}$$

where D is sediment particle size [m] and $\nu = 10^{-6}$ [m^2/s] is kinematic viscosity of water.

4.3.3. Efficiency criteria used for calibration and validation of simulated suspended sediment load

Calibration and validation of the suspended sediment load using the simulated equation (Eq.7) were performed using observed data of the sediment load and hydraulic characteristics recorded at the gauging stations over the course of 20 years (1994–2014). Eleven years of the pre-dam construction period (1994–2004) were used for calibration, and 10 years of the post-dam construction period (2005–2014) were used for validation. The model was calibrated by changing Manning's roughness coefficient between 0.01 and 0.02. The values of the roughness coefficient were selected based on the guideline of Schall et al. (2008). In which, the study sites are classified as "an alluvial sand bed, with no vegetation or plane bed with a Froude number less than unity". The calibration process selects the sediment particle size where the efficiency criteria reveal the most appropriate results.

Based on the recommendation of Moriasi et al. (2007), three efficiency criteria—the Nash-Sutcliffe efficiency (NSE), the percent bias (PBIAS), and the ratio of the root-mean-square error to the standard deviation of the measured data (RSR)—were used to evaluate the suspended sediment predictions. The sediment prediction can be judged as "satisfactory" for a monthly time step if NSE > 0.50, RSR ≤ 0.70, and PBIAS ≤ ±55%; "good" if 0.65 < NSE ≤ 0.75, 0.50 < RSR ≤ 0.60, and ±15% ≤ PBIAS ≤ ±30%; "very good" if 0.75 < NSE ≤ 1.00, PBIAS < ±15%, and 0.00 ≤ RSR ≤ 0.50; and "unsatisfactory" if NSE ≤ 0.50, RSR > 0.70 and PBIAS ≥ ±55% (Giang et al. 2017; Moriasi et al. 2007).

$$\mathrm{NSE} = 1 - \frac{\sum_1^n (SS_{obs} - SS_{cal})^2}{\sum_1^n (SS_{obs} - \overline{SS}_{obs})^2} \tag{4.9}$$

$$\mathrm{RSR} = \frac{\mathrm{RMSE}}{\mathrm{STDEV}^{\mathrm{obs}}} = \frac{\sqrt{\sum_1^n (SS_{obs} - SS_{cal})^2}}{\sqrt{\sum_1^n (SS_{obs} - \overline{SS}_{obs})^2}} \tag{4.10}$$

$$\mathrm{PBIAS} = \frac{\sum_1^n (SS_{obs} - SS_{cal})}{\sum_1^n SS_{obs}} \times 100, \tag{4.11}$$

where SS_{obs} is the observed daily sediment load, SS_{cal} is the calculated daily sediment load, $\overline{SS}_{obs}$ is the mean observed daily sediment load, and n is the total number of observations.

4.3.4. Electrical conductivity and total dissolved solids

Electrical conductivity is a measure of the capacity of water to conduct electrical current. Because conductivity is affected by temperature, it is reported at 25°C (i.e., the specific conductance). Because it is a volume measure of ionized solids, EC can be used to estimate TDS. The relationship between TDS and the specific conductance of water can be approximated by the following equation:

$$\mathrm{TDS} = k_e \times \mathrm{EC}, \tag{4.12}$$

where TDS is expressed in mg/L and the EC is in micro Siemens per centimeter at 25°C. The correlation factor k_e varies between 0.5 and 0.9 (typically 0.7) (Walton 1989). In this study, we used a correlation factor k_e of 0.65 (Thirumalini and Joseph 2009). The quantity of the dissolved solids transported by the river, expressed in kg/s, was determined by multiplying the concentration of the dissolved solids by the instantaneous discharge. The loading L_{DS}–Q curve for the dissolved solids was obtained from the analyzed data.

A long-term record of TDS was not available for the Ca River basin. Therefore, historical EC data were used to investigate changes in TDS after dam construction. At the research site, EC data for the Dua station were available once a month from 2000–2013. Additionally, to calculate the present TDS load, EC loggers (Model U24-001, HOBO®, Onset Computer Corporation, United States) and model U20-001-01 water level data loggers (HOBO®) were installed at the Dua station from July 1, 2016 through August 31, 2016 and at

the Yen Thuong station from June 23, 2016 through March 29, 2017. Electrical conductivity measurements were taken at 1-hour intervals. Water level data were used to calculate the discharge using the regime law.

4.4. RESULTS AND DISCUSSION

4.4.1. Hydraulic geometry characteristics at the cross-sectional scale

The relationship between hydraulic variables and discharge at the hydrological stations in the Ca River basin for the entire period of 1994–2014 is shown in Figure 4.2. The exponents and coefficients of the hydraulic geometry parameters at each station are listed in Table 4.1. At Dua station, the width of the river was constant (approximately 250 m throughout the discharge range); the depth and velocity increased progressively as power-law functions of the discharge. The depth increased with the discharge faster than the velocity ($h_o > u_o$). The scatter around the plots occurs both in the lower-flow regime and in the upper-flow regime; this scatter derives from measurement errors, analytical errors, random variations, and systematic changes to the channel (Knighton 1977, 1987). At Yen Thuong station, the velocity increased with the discharge faster than the depth, and the depth increased faster than the width ($u_o > h_o > b_o$) when the discharge was less than 2000 m^3/s. However, the depth increased with the discharge faster than the velocity ($h_o > u_o$); only the width remained constant around 410 m when the discharge exceeded 2000 m^3/s. A marked transition in river width and depth occurs at the Yen Thuong station, but the velocity of the river water is not affected for discharges exceeding approximately 2000 m^3/s.

Table 4.1. The exponents and coefficients of at-a-station hydraulic geometry parameters

	Exponents			Coefficients				
Stations	u_o	h_o	b_o	u_1	h_1	b_1	$u_o+h_o+b_o$	$u_1h_1b_1$
Dua	0.400	0.574	0.026	0.071	0.067	211.00	1.000	1.004
Yen Thuong ($Q < 2{,}000$ m^3/s)	0.431	0.332	0.236	0.046	0.316	68.54	0.999	0.996
Yen Thuong ($Q > 2000$ m^3/s)	0.396	0.523	0.079	0.058	0.080	217.04	0.998	1.007

Lewis (1966) and Knighton (1987) noted the type of discontinuity in hydraulic geometry (similar to Yen Thuong) related to lower-flow channelization. At higher flows, the rapid increase in water-surface width leads to a discontinuation of the flow regime, which is commonly associated with overtopping the channel banks and occupation of the adjoining floodplain. Therefore, a new relationship with the discharge develops (Knighton 1987;

Leopold and Maddock 1953). The discontinuity in hydraulic geometries can cause more than one break in the slope of the loading curve when the bank profile is highly irregular (Knighton 1987; Richards 1976). Ferguson (1986) concluded that "at-a-station hydraulic geometry" is a function of the shape of the channel.

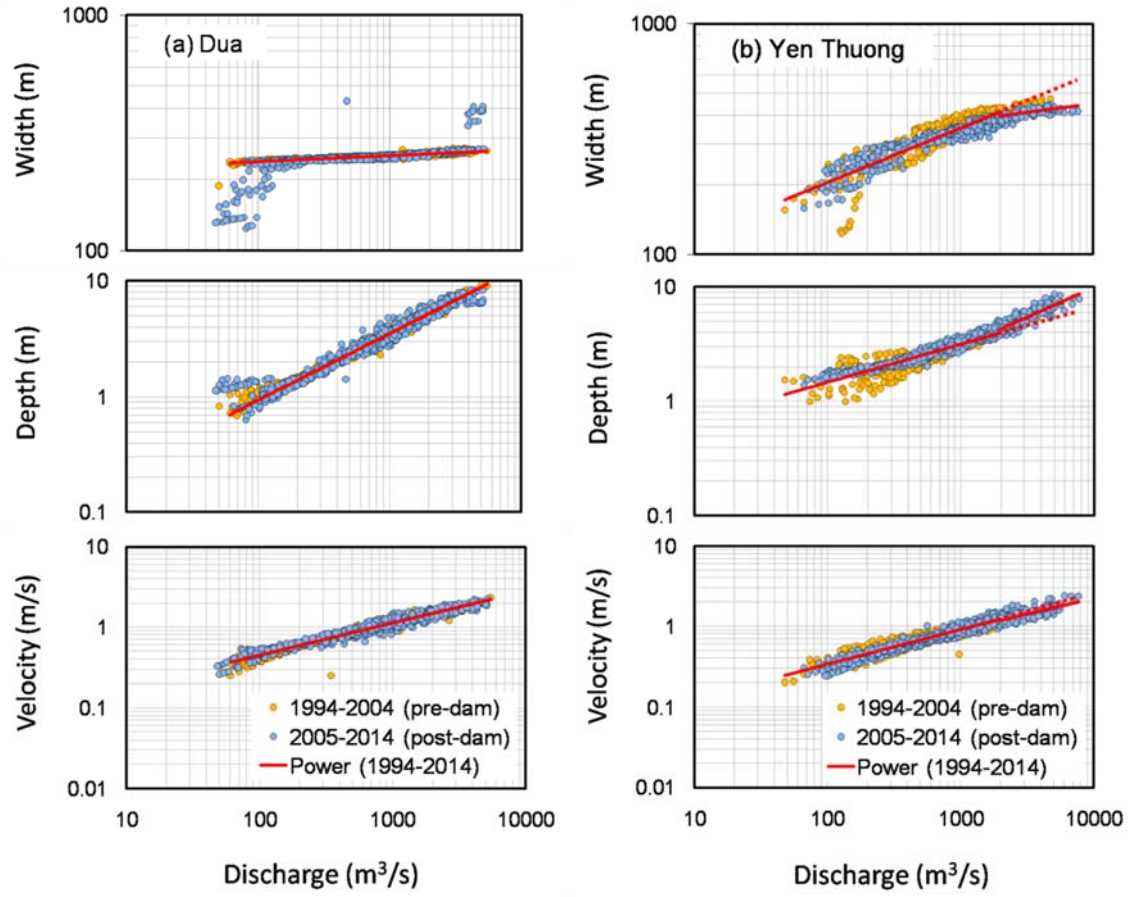

Figure 4.2. Relationship of width, depth, and velocity to discharge at Dua (a) and Yen Thuong (b)

Changes in the relationship among the hydraulic variables with discharge are compared between the pre-dam period (1994–2004) and the post-dam period (2005–2014) in Figure 4.2. The results reveal no significant changes in channel characteristics associated with dams at Dua station. However, an effect of dam construction on channel depth and width was observed at Yen Thuong station. The depth increased at discharges exceeding 2000 m^3/s during the post-dam period; the width of the river narrowed at the upper regime after dam construction. The depth during the post-dam period increased slightly, and there were fewer variations in lower discharges than during the pre-dam period.

4.4.2. Calibration and validation of the suspended sediment load

The parameters of hydraulic geometry listed in Table 4.1 can be used in Eq.7. The suspended sediment load is calculated as $L_{ss} = 0.54n^2w_s^{-1}Q^{1.46}$ for the Dua catchment and $L_{ss} = 0.02n^2w_s^{-1}Q^{1.85}$ if Q < 2,000 m^3/s and $L_{ss} = 0.31n^2w_s^{-1}Q^{1.49}$ if Q > 2,000 m^3/s for the Yen Thuong catchment.

To calibrate the suspended sediment load, the Manning roughness coefficient (n) is assumed to be a constant (0.015). The calibration process yielded the best values of the evaluation indices NSE, RSR, and PBIAS, which correspond to the optimal values of sediment diameters. The calibrated parameters were used to validate the post-dam period. Table 4.2 lists the calibrated and validated parameters. At Dua station, the best values of the NSE, RSR, and PBIAS indices were 0.708, 0.541, and 9% for a sediment particle size of 86 μm; the corresponding values were 0.591, 0.640, and 18% at Yen Thuong for a sediment particle size of 81 μm. The calibration process for sediment predictions can be judged as "satisfactory" to "very good" based on the procedure of Moriasi et al. (2007). The validated values of NSE, RSR, and PBIAS were 0.240, 0.872, and −26% at Dua and 0.090, 0.954, and −41% at Yen Thuong. Most of the evaluation index results were unsatisfactory for the post-dam period at both stations. A comparison of the observed and calculated sediment load (line 1:1 in Figure 4.3) indicates that the observed sediment decreased after dam construction.

Table 4.2. Calibration and validation results of the suspended sediment load at n = 0.015

	Indices	Dua	Yen Thuong	Validation 2005–2014
n*	*249*	*225*	*158*	*166*
D (μm)	86	86	81	81
NSE	0.708	0.240	0.591	0.090
RSR	0.541	0.872	0.640	0.954
PBIAS (%)	9	-26	18	-41

**Number of suspended solids samples*

Sediment discharge was numerically integrated using the log+linear profile in velocity and the equilibrium concentration profile described by Itakura and Kishi (1980). The coefficients and exponents were expressed using Manning's roughness coefficient, particle size, and the bed slope using the regression technique of Kazama et al. (2005). This technique was adapted for Dua and Yen Thuong along the Ca River. The results were obtained using the calibrated parameters n = 0.015 and D = 0.0008 m; the bed slope was assumed to be I = 1/20,000. Kazama et al. (2005) used the load-discharge (L-Q) relationship assuming that the

coefficient K and exponent P were functions of the slope, roughness, and particle size (I, n, and D).

$$Q_{ss} = KQ^{P+1} = KQ^{P}Q \tag{4.12}$$

Camenen and Larson (2008) derived the following equation using their reference concentration c_R based on laboratory results. This equation may be re-written using the diffusivity as $Ko = \eta\kappa u_* h$ and the Rouse number, $Z = w_s/\beta\kappa u_*$, where $\eta = \beta$ and $\beta\kappa = 1/15$.

$$q_{ss} = U_c c_R \frac{K_0}{w_s}\left\{1 - \exp\left[-\frac{w_s}{K_0}h\right]\right\} \tag{4.13a}$$

$$Q_{ss} = bq_{ss} = b\bar{u}c_R h\frac{\eta\kappa u_*}{w_s}\left\{1 - \exp\left[-\frac{w_s}{\eta\kappa u_*}\right]\right\} = \frac{C_R\{1-\exp[-Z]\}}{Z}Q \tag{4.13b}$$

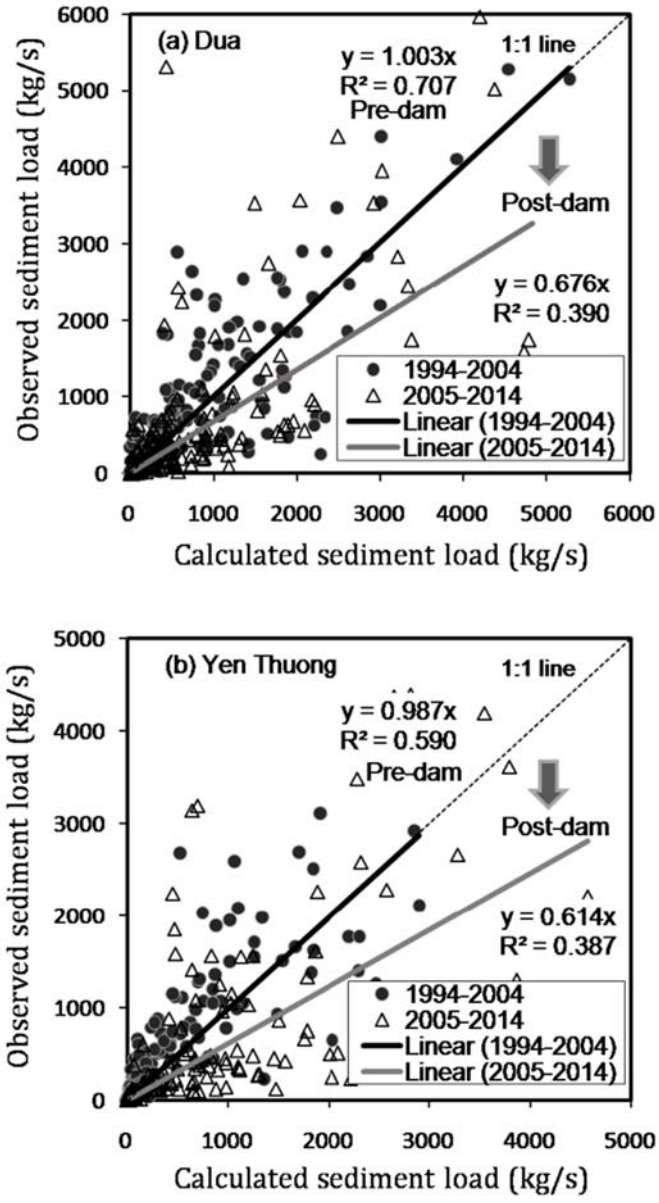

Figure 4.3. Comparison of observed and calculated sediment load at Dua (a) and Yen Thuong (b)

A steeper increase in the sediment loads was noted in two references (Figure 4.4). In the above calculations, particle size was fixed, which is why Camenen and Larson (2008) reported a strong decay in the lowest regime. Kazama et al. (2005) and Camenen and Larson (2008) showed a different dependence of the sediment load on the cross-sectional area and a slope of the curve exceeding 2. While Eq.(4.7) holds for slopes between 1.5 and 1.8, the logarithmic profiles and Manning equations are valid partly because of the different particle sizes according to the discharge and partly because of the departure from a steady and uniform flow. Those existing formulas are obtained from laboratory scale tests. However, the present study is fully dependent on the field data and likely reveals a variable particle size in the lower-flow regime with a shallower slope of the loading curve.

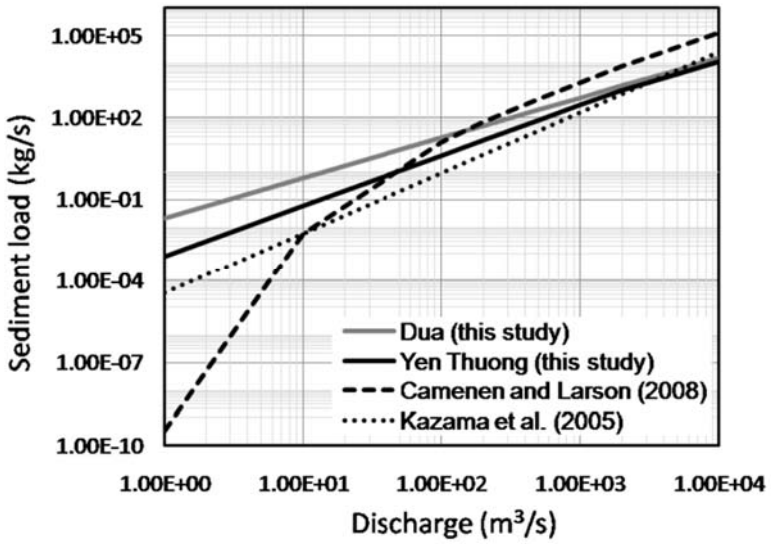

Figure 4.4. Loading curves at Dua and Yen Thuong compared with Kazama et al. (2005) and Camenen and Larson (2008)

4.4.3. Change in the relationship between sediment particle size and channel roughness

In the pre-dam period, the Manning roughness coefficient ranged from 0.01−0.02 $m^{-1/3}s$, and the sediment particle size was selected at the optimal values of the evaluation indices NSE, RSR and PBIAS. The obtained results of sediment size ranged from 57−124 μm at the Dua station and 54−118 μm at the Yen Thuong station. The calibration process was performed as trials in the post-dam period. The results of the NSE, RSR, and PBIAS indices were approximately 0.39, 0.781, and 14% at the Dua station and 0.39, 0.783, and 13% at the Yen Thuong station. The trade-off in n and D for the pre-dam and post-dam periods is demonstrated in Figure 4.5. The results indicate that a new correlation between sediment particle size and channel roughness was established. Dam construction significantly changed the sectional configuration and increased discharge of the river. These changes influenced

sediment particle size and channel roughness in the Ca River basin. The climate in the Ca River basin is tropical with monsoonal climate conditions, which results in large variations in annual runoff. Therefore, attaining the equilibrium concentration profile of suspended sediment for a given particle size is not easy. However, after the dams were constructed the river discharge somehow became regulated and the hydrograph was flattened; the coarsest particles became immobile and the finest particles moved during the dry season. The discharge range (minimum to maximum discharge) narrowed, which is one possible reason why the riverbed got coarser. This situation may have resulted in a significant increase in the roughness (Chien 1985). A similar tendency was reported by Leopold and Maddock (1953) in a laboratory.

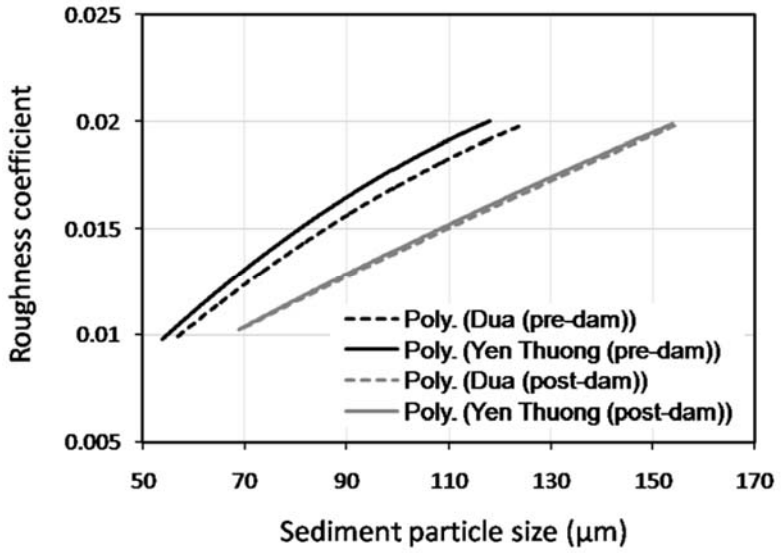

Figure 4.5. The relationship between sediment particle size and channel roughness during the pre-dam and post-dam periods

4.4.4. Impact of a reservoir on suspended sediment yield

Observed sediment loading curves L_{ss}–Q before and after dam construction in the Ca River basin are presented in Figure 4.6. The sediment loading curve decreases from $L_{ss}=0.0036\times Q^{1.6659}$ to $L_{ss}=0.0012\times Q^{1.76}$ at Dua station and from $L_{ss}=0.0027\times Q^{1.704}$ to $L_{ss} = 0.0027\times Q^{1.591}$ at Yen Thuong station. The annual suspended sediment load was calculated using sediment loading curves for the pre-dam and post-dam periods. The mean annual suspended sediment load decreased by 20% from 4.0×10^6 tons to 3.2×10^6 tons at Dua station and by more than 40% from 6.6×10^6 tons to 3.7×10^6 tons at Yen Thuong station after dam construction. In the pre-dam period, Yen Thuong received about 60% of the suspended sediment from the Upper Dua basin. During the post-dam period, this fraction increased to 86%. The Upper Dua basin covers an area of 20,800 km^2, and the basin between Dua and Yen

Thuong (Lower Dua basin) covers an area of 2200 km^2. The mean annual sediment yield of the Upper Dua basin decreased by 20% from 194 tons/yr/km^2 to 152 tons/yr/km^2. The annual sediment yield of the Lower Dua basin decreased by more than 80% from 1,156 tons/yr/km^2 to 231 tons/yr/km^2. These results indicate that the rate of sediment loss following impoundments in the lower basin was higher than in the upper basin.

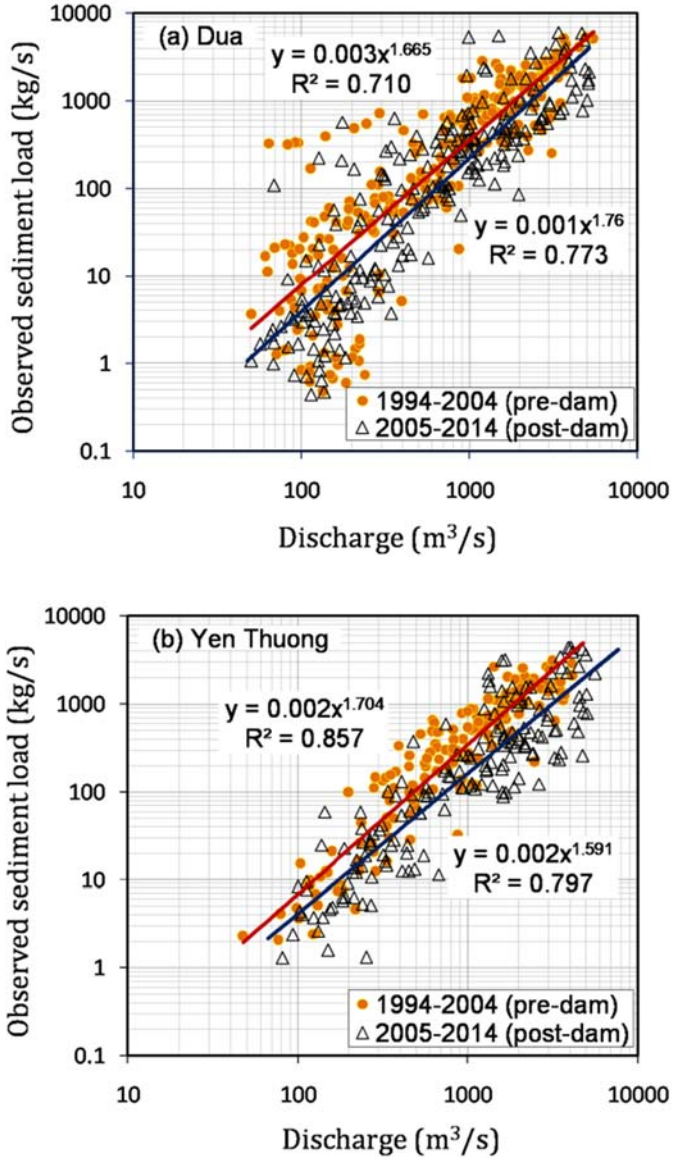

Figure 4.6. Observed SS load during the pre-dam and post-dam periods at Dua (a) and Yen Thuong (b)

4.4.5. Long-term TDS yields and changes in the TSS-to-TDS ratio

Long-term EC and water level data at the Dua station are presented in Figure 4.7. Electrical conductivity ranged between 88 and 219 µS/cm, and it gradually increased from 2000−2013. A negative relationship was observed between EC and water level during runoff peaks. The long-term EC data were converted to TDS concentration for the pre- and post-dam

periods. The loading curve of TDS (L_{DS}–Q) in Figure 4.8 shows the results of a dissolved solid load in the pre-dam and post-dam periods at the Dua station combined with the TDS load converted from the logger data at both stations. Similar loading curves for TDS were obtained for the pre- and post-dam periods and for the logger data at the Dua station. Therefore, the TDS load, on average, was not affected significantly by dam construction. However, this comparison is a very rough estimate.

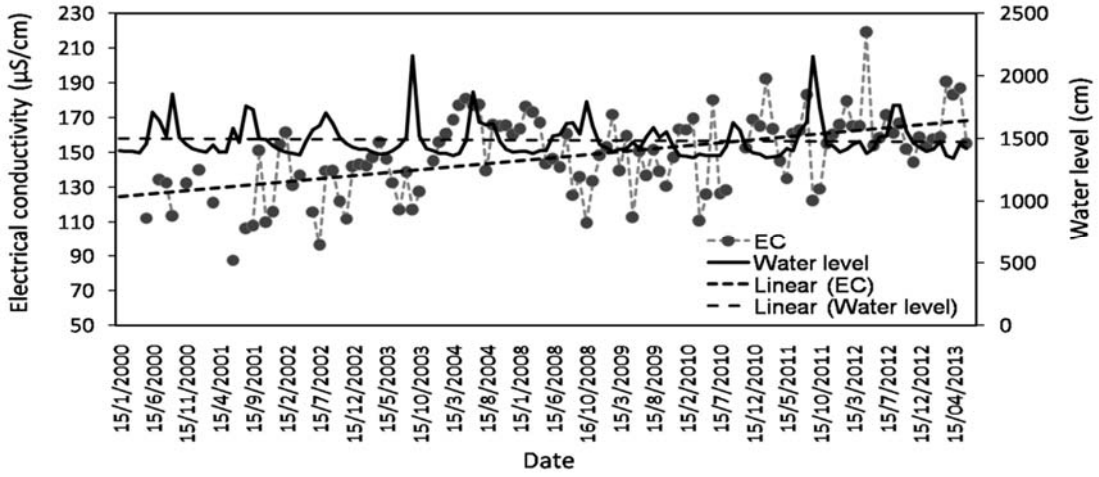

Figure 4.7. Long-term electrical conductivity at the Dua station

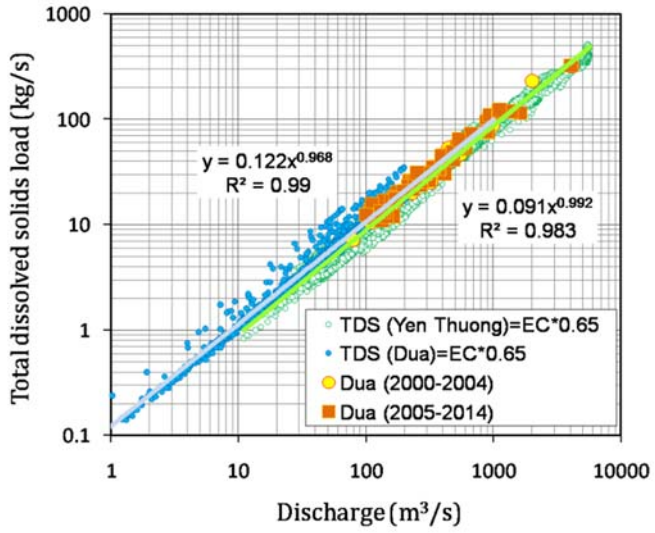

Figure 4.8. Loading curve of total dissolved solids at the Dua station

The dissolved solid loads increased with increasing river flow as a power function $L_{DS}=0.122\times Q^{0.968}$ at Dua and $L_{DS}=0.091\times Q^{0.992}$at Yen Thuong. Long-term annual TDS loads were calculated by applying an observed TDS loading curve. The TDS load ranged between 3.6×10^5 and 2.0×10^6 tons/yr at Dua and between 6.1×10^5 and 2.4×10^6 tons/year at Yen Thuong during the time period 1994–2014. The average annual TDS load was 1.3×10^6 tons at

Dua and 1.5×10^6 tons at Yen Thuong. On average, Yen Thuong received more than 80% of its TDS load from the Dua basin. The mean annual specific yield of TDS in the Upper Dua basin was 61 tons/yr/km^2; the corresponding value in the Lower Dua basin (between Dua and Yen Thuong) was 124 tons/yr/km^2 for the entire period (1994–2014). The TDS yield in the Lower Dua basin was two-fold higher than that of the Upper Dua basin.

The annual TSS-to-TDS ratio ranged from 1.3−4.8, with an average of 2.7 at Dua station, and from 1.3−6.9, with an average of 3.2 at Yen Thuong station over the time period 1994–2014. The average TSS-to-TDS ratio decreased from 3.0 to 2.3 at Dua and from 4.1 to 2.2 at Yen Thuong after dam construction. According to the classification of Milliman and Farnsworth (2011), the Ca River basin is a sediment-dominated river (TSS/TDS > 2). The TSS-to-TDS ratio at the Yen Thuong station was higher than that at the Dua station during the pre-dam period. However, reservoir construction caused a change in the load of TDS and TSS into rivers, resulting in an altered TSS-to-TDS ratio. It has been reported that dams decreased sediment loads and caused a shift from a sediment-dominated to dissolved-dominated river in many rivers worldwide (Milliman and Farnsworth 2011).

4.5. CONCLUSIONS

Suspended sediment transport at two hydrological stations, Dua and Yen Thuong, in the Ca River basin was simulated using semi-empirical forms based on the regime curves for width, depth, and average velocity with roughness coefficient and bulk sediment concentration formulas. Three efficiency criteria—NSE, PBIAS, and RSR—were used to evaluate the suspended sediment predictions during the pre-dam (1994–2004) and post-dam (2005–2014) periods. The comparison of observed and calculated sediment load indicated that the observed sediment decreased after dam construction. Suspended sediment transport was then obtained as a loading curve in terms of the *L–Q* equations and compared with theoretical methods presented in the literature. The exponents of the loading curve in this study ranged between 1.46 and 1.85; values exceeding 2.00 have been noted in the literature.

One of the effects of dam construction that we noted was a change in the relationship between Manning's roughness coefficient and sediment particle size. This result was manifested at both stations, and sediment transport was reduced after dam construction, which resulted in reservoir sedimentation. The fraction of lighter solids was suggested to have increased. The mean annual suspended sediment load decreased by 20% from 4.0×10^6 tons to 3.2×10^6 tons at the Dua station and by more than 40% from 6.6×10^6 tons to 3.7×10^6 tons at the Yen Thuong station after dam construction. A power-law function with exponents of 0.968 and 0.992 of dissolved solid load was used to calculate the long-term annual TDS at

Dua and Yen Thuong, respectively. The TDS load ranged between 0.4 and 2.0 million tons per year at the Dua station and between 0.6 and 2.4 million tons per year at the Yen Thuong station over the time period 1994–2014. The reduction in TSS after dam construction led to a decrease in the TSS-to-TDS ratio from 3.0 to 2.3 at the Dua station and from 4.1 to 2.2 at the Yen Thuong station.

REFERENCES

Amos P, Veale B, Thai NC, Read S (2017) Improving dam and downstream community safety in Vietnam. Hydropower Dams 1

Andrews ED (1986) Downstream effects of Flaming Gorge Reservoir on the Green River, Colorado and Utah. Geol Soc Am Bull 97: 1012–1023

Brinkmann WLF (1989) Hydrology. In: Lieth H, Werger MJA (eds) Tropical rain forest ecosystems: Biogeographical and ecological studies. Elsevier, Amsterdam, pp 89–98

Camenen B, Larson M (2008) A general formula for noncohesive suspended sediment transport. J Coast Res 24(3):615–627

Celik I, Rodi W (1991) Suspended sediment-transport capacity for open channel flow. J Hydraul Eng 117(2): 191–204

Chien N (1985) Changes in river regime after the construction of upstream reservoirs. Earth Surf Process Landf 10: 143–159

Chikamori H, Heng L, Daniel T (eds) (2012) Catalogue of rivers for Southeast Asia and the Pacific–Volume VI. UNESCO-IHP Regional Steering Committee for Southeast Asia and the Pacific

Eiriksdottir ES, Oelkers EH, Hardardottir J, Gislason SR (2017) The impact of damming on riverine fluxes to the ocean: A case study from Eastern Iceland. Water Res 113: 124–138

Ferguson RI (1986) Hydraulics and hydraulic geometry. Prog Phys Geogr 10: 1–31

Friedl G, Wüest A (2002) Disrupting biogeochemical cycles–Consequences of damming. Aquat Sci 64(1): 55–65

Giang PQ, Giang LT, Toshiki K (2017) Spatial and temporal responses of soil erosion to climate change impacts in a transnational watershed in Southeast Asia. Climate 5(1)

Habini M (1994) Sediment transport estimation methods in river systems. Dissertation, University of Wollongong. Retrieved from http://ro.uow.edu.au/theses/1263/

Humborg C, Ittekkot V, Cociasu A, Bodungen B V (1997) Effect of Danube River dam on Black Sea biogeochemistry and ecosystem structure. Nature 386: 385–388

Itakura T, Kishi T (1980) Open channel flow with suspended sediments. J Hydraul Div 106(8): 1325–1343

Kazama S, Suzuki K, Sawamoto M (2005) Estimation of rating-curve parameters for sedimentation using a physical model. Hydrol Process 19: 3863–3871

Knighton AD (1977) Short-term changes in hydraulic geometry. In: Gregory KJ (ed) River channel changes. Wiley, Chichester, pp 101–119

Knighton AD (1987) Streamflow characteristics of northeastern Tasmania: II. Hydraulic geometry. Pap Proc Roy Soc Tas 121: 125–135

Leopold LB, Maddock T (1953) The hydraulic geometry of stream channels and some physiographic implications. US Government Printing Office, Washington

Lewis LA (1966) The adjustment of some hydraulic variables at discharges less than one cfs. Prof Geogr 18(4): 230–234

Meybeck M (2003) Global analysis of river systems: from Earth system controls to Anthropocene syndromes. Philos Trans R Soc Lond B Biol Sci 358(1440): 1935–1955

Milliman JD, Farnsworth KL (2011) River discharge to the coastal ocean: a global synthesis. Cambridge University Press, New York

Moriasi DN, Arnold JG, Van Liew MW, Binger RL, Harmel RD, Veith TL (2007) Model evaluation guidelines for systematic quantification of accuracy in watershed simulations. Trans ASABE 50(3): 885–900

Richards KS (1976) Complex width-discharge relations in natural river sections. Geol Soc Am Bull 87(2): 199–206

Schall JD, Richardson EV, Morris JL (2008) Introduction to highway hydraulics: Hydraulic design series no 4. US Department of Transportation, Federal Highway Administration, Washington

Thirumalini S, Joseph K (2009) Correlation between electrical conductivity and total dissolved solids in natural waters. Malays J Sci 28(1): 55–61

Walton NRG (1989) Electrical conductivity and total dissolved solids–What is their precise relationship? Desalination 72(3): 275–292

Xu J (2007) Trends in suspended sediment grain size in the upper Yangtze River and its tributaries, as influenced by human activities. Hydrol Sci J 52(4): 777–792

Yang Y, Zhang M, Zhu L, Liu W, Han J, Yang Y (2017) Influence of large reservoir operation on water-levels and flows in reaches below dam: Case study of the Three Gorges Reservoir. Sci Rep 7(1)

CHAPTER 5. GEOCHEMISTRY AND SEDIMENT: WEATHERING PROCESS, SOLUTE-DISCHARGE RELATIONSHIP, AND RESERVOIR IMPACT

5.1. INTRODUCTION

The natural chemical compositions and transport fluxes in rivers depend on multiple environmental factors such as sources (lithosphere, atmosphere, biosphere), sinks (vegetation uptake, settling), rate-controlling factors (temperature, water circulation), and drainage basin area (Meybeck 1994; Milliman and Farnsworth 2011). Atmospheric pollution and human activity can have significant effects on the natural geochemistries of river basins (Chetelat et al. 2008; Li et al. 2009; Li and Zhang 2008; Roy et al. 1999). Detailed geochemical studies have quantified major ion compositions (Li and Zhang 2008; Maharana et al. 2015), weathering processes (Chetelat et al. 2008; Sarin et al. 1989), long-term fluxes (Negrel et al. 2007; Sarin et al. 1989), and controlling factors in solute exports from various scales of basins (Godsey et al. 2009; Musolff et al. 2015). Some have researched natural river geochemistry, where basins with minimal human activity, such as hilly headwater basins (Bruijnzeel 1983) and unpolluted or less-polluted river basins (Meybeck 1994), were considered. However, establishing natural background values is challenging because most major rivers are already directly polluted or exposed to long-range transport of atmospheric pollutants (Meybeck and Helmer 1989).

Rivers in Vietnam, like many other rivers around the world, have been impacted by economic development. Reservoirs of various size have been constructed along the rivers for power generation, water supply, and flood control (Amos et al. 2017). In addition, other anthropogenic activities (e.g., intensive agriculture, land-use change, and industrial development) can have significant impacts on how natural river materials move. However, geochemical data for Vietnamese rivers are sparse. Thus, we investigated the geochemistry of the Ca River, one of the large basins in north-central Vietnam, covering an area of 27,200 km^2. Major ion chemistries were determined at sites upstream of the reservoirs, which were primarily under forest cover, and at sites mid- and downstream, below the reservoirs. Weathering processes controlling the major geochemistry were also determined. Additionally, variations in the concentrations of major chemical ions and suspended solids in the discharge were investigated.

5.2. STUDY AREA

The Ca River is an international river located between 18°15'00"N to 20°10'30"N and 103°45'20"E to 105°15'20"E (Figure 5.1). The basin covers 27,200 km^2, including 17,730

km^2in Vietnam's territory and 9470 km^2 in Laos. The main river originates from Mt. Muong Khut and Muong Lap (1800 to 2000 m) in Laos, flows from northwest to southeast, enters into the Nghe An, Thanh Hoa, and Ha Tinh provinces of Vietnam, and flows out to the Eastern Sea at the Hoi estuary. Total river length is 531 km, of which 170 km runs through Laos and 361 km is in Vietnam. Forests in the Ca River basin are largely located upstream of three Laos provinces (Bolikhamxay, Xieng Khouang, and Houaphanh). In Vietnam, forests are concentrated in north, northwest, and southwest of the basin at elevations of 150 to 1500 m (IWRP 2012). The catchment is covered primarily by forest (44%) and agricultural crops (18%) (Chikamori et al. 2012). Area soils are formed from parent rocks, Ferralsol in particular (83.51%) (IWRP 2012; Nauditt and Ribbe 2017). Other soil types are Fluvisol and Acrisol. The Ca River basin is located in a monsoon climate, and rainfall is distributed over the year, which has two distinct seasons: the dry season and the rainy season. In the upper reaches of the river, the rainy season is from May to October, but in downstream, it is from June to November. Average annual precipitation in the basin is 1100 to 2500 mm.

Multiple reservoirs have been constructed in the Ca River basin, namely Ban Ve, Khe Bo, Thac Muoi, and Sao reservoirs. These multi-purpose reservoirs are used for hydropower generation, water supply, irrigation, and flood and drought control. Ban Ve is the largest among them and is located at approximately 100 m elevation. Its gross capacity is 1835×10^6 m^3, and its effective capacity is 1383×10^6 m^3.

Samples were obtained from the main stream of the Ca River at My Ly (104°18'54"E and 19°36'51"N), Dua (105°02'20"E and 18°59'20"N), and Yen Thuong ($105^0$23'00"E and $18^0$41'10"N). My Ly is located approximately 215 m above the Ban Ve reservoir (70 km). It covers 1190 km^2 or 4.4% of the total drainage basin. Located in the high mountains and covered primarily by forest, the My Ly basin is sparsely populated and is subject to little human impact. Both Dua and Yen Thuong are downstream of all reservoirs, covering 20,800 km^2 and 23,000 km^2 (76.5% and 84.6% of the river basin), respectively. Both are strongly influenced by human activity (e.g., agriculture and mining activities). Additionally, water storage and reservoir operations impact the Ca River and its resources.

5.3. SAMPLING AND ANALYTICAL METHODS

From August 2017 to July 2018, 121 water samples were collected from three hydrological stations in the main stream of the Ca River basin. During the flood season, water samples were collected four to six times monthly, and during the dry season, they were collected one to four times monthly. Samples were representative of the range of discharge rates.

Each sample of 2 L, collected from an average depth of 10 cm at the river bank, was placed in high-density polyethylene containers then immediately cooled and maintained at a low temperature until analysis. Concentrations of the major cations (Ca^{2+},Mg^{2+}, Na^{+}, and K^{+}), anions (HCO_3^-, SO_4^{2-}, Cl^-, NO_3^-, and PO_4^{3-}), and dissolved silica (SiO_2) were determined in the laboratory. Cation and most anion concentrations were found using ion chromatography (Shimadzu, Japan). Dissolved silica and phosphate were measured using a DR900 (HACH) colorimeter. Water samples were filtered through pre-washed 0.45-µm Millipore membrane filters before ion concentrations were determined. Additionally, the concentration of suspended solids was determined by filtering 100 mL sample through a 0.45-µm membrane filter (Whatman). Finally, the total concentration of all dissolved solids was the sum of the major elements plus dissolved silica.

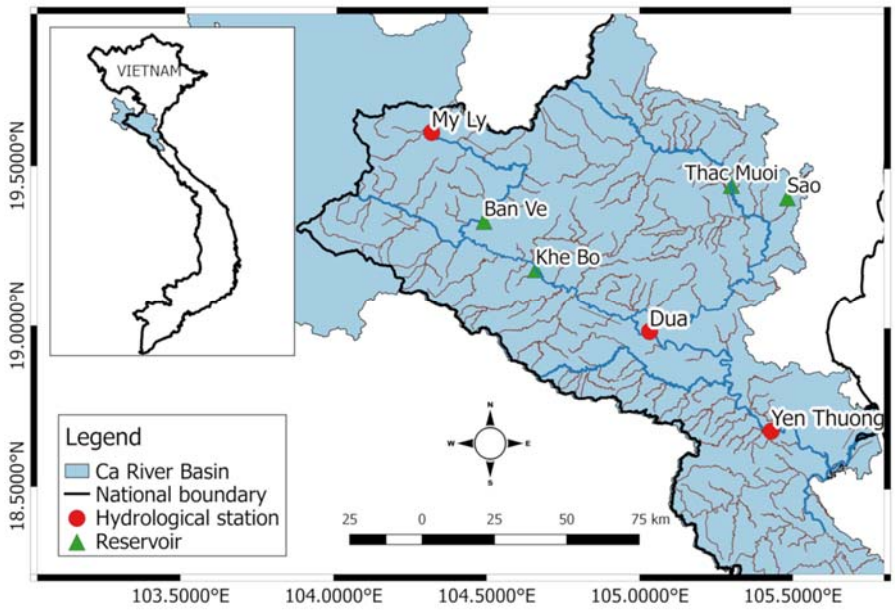

Figure 5.1. Map of the Ca River basin

5.4. RESULTS AND DISCUSSION

5.4.1 The contribution of chemical compositions

The concentration of each major chemical in the main stream of the Ca River basin is given in Table 5.1. Total dissolved solids (TDS) varied from 77 to 205 mg/L, averaging 144 mg/L, higher than the world average, 100 mg/L (Milliman and Farnsworth 2011). The average value for TDS is comparable to that reported for the Hong River (176 mg/L) in Vietnam, but it is lower than that reported for the Son River in India (227 mg/L) and the Upper Han River in China (248 mg/L) (Li and Zhang 2008; Maharana et al. 2015; Moon et al. 2007). Compared with the rivers draining in areas dominated by silicate rock, such as the

upper Ganjiang River (63 mg/L) and rivers in the Southeast Coastal Region of China (75.2 mg/L), TDS in the Ca River is much higher (Liu et al. 2018; Ji and Jiang 2012). However, it is much lower compared to the Huanghe River (557 mg/L) and Tarim River (1000 mg/L), both of which drain in areas dominated by evaporite dissolution (Fan et al. 2014; Xiao et al. 2012). Bedrock lithology plays a critical role in controlling the character and quantity of the total delivered (Meybeck 1987; Milliman and Farnsworth 2011). Human activity also significantly influences TDS values (e.g., in the Liao River of China [400 mg/L] and several European rivers [Ding et al. 2016; Milliman and Farnsworth 2011]).

The total cationic charge ($Tz^+ = 2Ca^{2+} + 2Mg^{2+} + K^+ + Na^+$) ranged from 1145 to 2981 μeq/L, averaging 2119 μeq/L. The total anionic charge ($Tz^- = HCO_3^- + 2SO_4^{2-} + Cl^- + NO_3^- + 3PO_4^{3-}$) ranged from 811 to 2271 μeq/L, averaging 1567 μeq/L. The extent of $Tz^+ - Tz^-$ charge imbalance, characterized by the normalized inorganic charge balance ($NICB = (Tz^+ - Tz^-)/Tz^+$), is related to the contributions of other anions (Li et al. 2009; Ji and Jiang 2012).

Calcium was the dominant cation, ranging in concentration from 381 to 1005 μM, accounting for an average of 62.0% of the total cation charge. Magnesium followed, ranging from 102 to 368 μM, accounting for an average of 23.2% of the total cation charge, and then sodium (12.3%) and potassium (2.4%). Bicarbonate was the dominant anion, ranging from 600 to 2039 μM, accounting for 84.4% of the total anion charge. Chloride and sulfate together comprised 12.6% of the total anion charge in nearly equal proportions. Nitrate and phosphate contributed negligible proportions (2.7% and 0.3%, respectively).

Dissolved Si ranged in concentration from 133 to 250 μM, averaging 202 μM, comprising an average of 8.6% of the TDS. It ranked third in abundance after HCO_3^- (55.8%) and Ca^{2+} (18.3%). Compared to other major ions, dissolved Si was relatively independent of lithology, remaining constant between 80 and 160 μmol/L SiO_2(except in streams draining volcanic rocks, where it reaches 350 μmol/L SiO_2) (Meybeck 1987). Dissolved Si content is, however, controlled by the climate (temperature and rainfall) (White and Blum 1995).

Table 5.1. Chemical compositions of the rivers in the Ca River basin

Stations	Date	Discharge	Na^+	K^+	Ca^{2+}	Mg^{2+}	Cl^-	SO_4^{2-}	HCO_3^-	NO_3^-	PO_4^{3-}	SiO_2	NIBC	TSS
		m^3/s	mg/l	mg/l	mg/l	mg/l	mg/l	mg/l	mg/l	mg/l	mg/l	mg/l		mg/l
My Ly	13/08/2017	172	4.65	1.30	30.43	7.89	1.15	4.28	120.80	-	0.13	12	0.12	54
	20/08/2017	154	13.87	1.73	18.74	6.68	7.93	6.00	97.60	-	0.16	13	0.08	41
	27/08/2017	198	14.20	2.76	24.51	7.90	12.24	6.76	107.40	-	0.14	12	0.12	81
	03/09/2017	152	6.69	1.70	29.40	7.37	2.89	4.16	95.16	-	0.17	13	0.28	183
	10/09/2017	148	6.29	1.83	28.86	8.55	2.82	5.45	101.30	-	0.15	13	0.25	59
	16/09/2017	400	5.97	1.83	22.74	6.74	3.11	4.61	100.00	2.82	0.25	13	0.06	576
	17/09/2017	380	4.39	1.64	30.54	6.92	2.19	5.93	118.30	2.54	0.19	12	0.07	502

	24/09/2017	108	5.46	2.30	24.34	5.45	3.69	5.78	102.50	1.78	0.13	13	0.01	46
	01/10/2017	128	7.67	1.39	26.86	8.87	3.79	3.86	96.38	0.85	0.17	13	0.27	25
	08/10/2017	132	13.63	3.16	27.55	7.67	10.65	6.14	91.50	10.11	0.17	13	0.22	46
	22/10/2017	348	11.78	1.78	28.42	6.94	5.45	9.46	93.94	1.06	0.20	13	0.25	15
	05/11/2017	328	8.19	1.63	26.99	7.56	3.85	5.43	96.38	2.23	0.12	12	0.22	5
	12/11/2017	132	4.65	1.17	27.82	7.09	1.01	4.56	97.60	0.38	0.19	13	0.21	6
	19/11/2017	132	6.65	2.31	28.51	8.66	2.32	5.43	93.94	0.93	0.12	13	0.30	5
	26/11/2017	130	4.93	1.31	28.23	7.64	0.62	4.97	97.60	0.54	0.11	14	0.24	7
	03/12/2017	130	6.77	2.23	26.98	8.27	3.08	5.87	96.38	2.14	0.13	13	0.23	3
	10/12/2017	132	6.24	1.25	23.11	7.33	0.57	5.32	90.28	5.39	0.12	13	0.18	7
	17/12/2017	132	8.38	2.20	25.04	7.24	3.16	4.87	96.38	2.27	0.10	14	0.20	9
	24/12/2017	129	4.57	1.21	24.65	6.11	1.97	4.83	93.94	1.29	0.04	13	0.12	3
	30/12/2017	129	5.64	1.90	29.36	7.72	3.25	5.50	97.60	1.87	0.15	13	0.23	12
	21/01/2018	80	4.76	1.62	27.79	5.23	2.47	4.25	79.30	4.05	0.19	12	0.26	5
	28/01/2018	50	11.08	1.68	29.94	8.95	6.60	6.28	98.82	6.30	0.08	12	0.26	7
	04/02/2018	42	9.54	1.87	28.24	8.92	5.97	6.52	96.38	2.43	0.11	13	0.26	3
	04/03/2018	40	6.35	1.93	26.38	6.44	3.70	3.94	102.50	3.12	0.04	13	0.12	4
	11/03/2018	40	7.12	1.78	31.39	8.20	3.39	5.27	102.50	1.98	0.11	13	0.26	23
	01/04/2018	40	10.83	2.49	30.75	8.15	4.98	6.28	97.60	1.02	0.10	14	0.31	39
	08/04/2018	40	5.06	2.14	31.51	8.03	1.43	5.90	97.60	1.48	0.23	14	0.28	360
	16/04/2018	72	8.62	2.01	32.65	8.33	4.50	5.06	98.82	3.27	0.09	12	0.30	265
	29/04/2018	48	13.17	3.08	27.06	7.53	8.85	6.62	87.84	6.09	0.17	14	0.26	632
	06/05/2018	94	5.96	2.27	26.77	7.29	2.00	4.89	95.16	2.39	0.20	12	0.22	410
	13/05/2018	72	5.02	2.13	34.24	7.74	1.49	6.20	98.82	1.01	0.23	15	0.31	414
	27/05/2018	60	5.15	2.17	30.41	6.07	2.28	4.94	81.74	1.64	0.36	12	0.33	200
	03/06/2018	160	6.70	2.31	34.31	8.37	3.41	5.67	109.80	3.45	0.40	12	0.24	536
	17/06/2018	240	4.49	3.14	40.27	8.46	2.00	6.12	124.40	2.37	0.33	13	0.24	3727
	24/06/2018	87	4.29	1.47	35.91	8.02	0.94	5.25	112.20	0.96	0.11	12	0.25	338
	08/07/2018	72	5.25	1.64	28.60	7.51	1.23	2.62	103.70	0.31	0.12	12	0.22	197
	16/07/2018	160	5.59	2.78	23.19	5.50	3.88	5.97	106.10	2.57	0.08	12	-0.05	387
	22/07/2018	2100	3.33	1.27	26.42	5.95	2.86	7.35	89.06	5.35	0.16	12	0.10	2310
Dua	06/08/2017	869	4.16	1.75	23.39	4.35	2.68	2.87	84.18	-	0.20	12	0.13	77
	14/08/2017	463	3.47	1.45	23.89	5.12	1.24	3.20	85.40	-	0.19	13	0.16	57
	20/08/2017	860	8.65	1.97	23.04	4.84	5.47	3.88	63.44	-	0.13	12	0.35	106
	27/08/2017	882	3.76	1.83	26.77	4.98	2.43	3.30	78.08	-	0.19	11	0.27	85
	04/09/2017	565	3.99	1.54	21.73	5.23	2.30	3.29	70.76	-	0.15	12	0.25	58
	10/09/2017	562	3.94	1.43	24.98	5.49	1.92	3.41	73.20	-	0.18	11	0.30	42
	17/09/2017	2688	3.77	1.83	18.41	3.86	2.37	3.26	51.24	3.60	0.25	10	0.28	621
	24/09/2017	610	4.59	2.10	23.47	5.39	2.06	4.11	75.64	3.35	0.15	12	0.23	62
	01/10/2017	749	10.14	1.63	26.80	5.78	10.82	3.06	81.74	2.14	0.14	13	0.24	33
	08/10/2017	1241	6.13	2.25	20.97	4.55	4.72	3.60	63.44	5.79	0.20	12	0.23	174
	10/10/2017	1772	3.45	1.70	18.75	3.09	2.51	2.71	54.90	3.91	0.19	11	0.21	395
	11/10/2017	3564	2.91	1.77	16.98	3.40	2.41	2.51	61.00	3.81	0.18	12	0.09	411
	12/10/2017	4393	2.55	1.82	16.08	2.89	2.00	2.58	43.90	4.43	0.24	9	0.24	465
	22/10/2017	700	8.65	1.76	26.22	6.37	5.06	5.68	78.08	3.78	0.17	14	0.29	40
	05/11/2017	336	8.22	1.89	27.37	6.22	4.34	3.99	80.52	3.42	0.10	13	0.31	17
	12/11/2017	440	9.51	2.30	27.86	6.68	5.99	4.34	84.18	3.12	0.16	14	0.30	8
	20/11/2017	283	4.80	1.97	27.70	6.18	1.97	4.20	78.08	2.40	0.13	13	0.32	36
	26/11/2017	246	3.73	1.45	24.71	5.30	0.97	4.21	80.52	2.38	0.14	14	0.21	17
	03/12/2017	259	4.65	1.59	24.31	5.39	1.92	3.75	75.64	2.69	0.14	14	0.25	12
	10/12/2017	494	4.28	1.57	23.88	5.30	1.71	3.73	84.18	3.00	0.11	13	0.16	10
	18/12/2017	195	14.05	4.47	27.62	7.82	8.94	10.08	79.30	5.97	0.08	13	0.32	8
	24/12/2017	170	4.98	1.45	24.14	5.45	2.22	4.41	81.74	2.08	0.09	13	0.20	4
	31/12/2017	240	8.64	2.55	25.80	7.01	7.62	4.84	78.08	4.61	0.13	13	0.27	5
	21/01/2018	289	5.66	1.59	27.85	6.08	2.45	4.00	81.70	1.95	0.12	11	0.30	9
	27/01/2018	169	8.85	2.20	30.37	7.28	6.93	4.72	93.94	2.93	0.06	11	0.26	12
	04/02/2018	154	4.37	1.51	28.35	6.04	1.23	4.37	86.62	1.42	0.14	13	0.27	8
	04/03/2018	56	4.65	1.86	27.27	5.55	2.68	3.75	87.84	2.82	0.04	12	0.21	8
	11/03/2018	185	4.43	1.62	30.77	6.45	1.53	4.56	87.84	1.97	0.13	12	0.30	8
	02/04/2018	117	10.39	2.39	31.33	7.77	5.79	5.52	86.60	3.27	0.08	12	0.35	3
	07/04/2018	345	4.50	1.62	31.64	6.29	2.37	4.45	86.62	1.64	0.08	12	0.31	139
	17/04/2018	300	5.59	1.86	31.70	6.80	2.74	4.34	86.62	2.11	0.10	12	0.33	6
	01/05/2018	275	4.31	1.92	28.14	5.79	2.10	4.34	80.52	1.81	0.09	13	0.29	14
	06/05/2018	294	7.28	2.04	28.62	6.64	4.79	3.60	73.20	3.80	0.23	12	0.37	76
	13/05/2018	339	8.69	2.21	27.00	5.59	5.69	4.66	74.42	4.46	0.19	12	0.31	44
	20/05/2018	356	4.67	2.01	28.29	6.38	2.14	5.20	73.00	2.21	0.19	11	0.36	557
	27/05/2018	252	4.38	2.03	29.49	5.64	2.09	3.05	76.86	1.05	0.20	11	0.35	9

	03/06/2018	319	5.87	2.71	29.79	5.79	3.70	4.27	84.18	1.43	0.35	11	0.30	13
	17/06/2018	316	6.95	2.37	27.14	5.46	4.99	4.70	73.20	2.63	0.13	13	0.31	157
	24/06/2018	420	4.08	1.84	25.76	5.22	1.92	3.90	70.76	1.40	0.13	12	0.32	40
	08/07/2018	455	8.85	2.34	30.31	6.70	4.82	5.43	84.18	2.30	0.19	12	0.33	13
	16/07/2018	747	5.69	1.36	22.24	2.87	5.69	3.29	84.18	2.26	0.10	11	-0.01	72
	22/07/2018	4210	2.22	1.79	20.71	4.30	1.26	4.58	70.76	3.83	0.26	11	0.11	867
Yen	06/08/2017	752	3.39	1.44	21.74	4.15	1.51	3.27	74.42	-	-	-	0.17	158
Thuong	14/08/2017	430	3.39	1.60	22.97	4.69	1.72	3.20	86.62	-	0.23	12	0.10	77
	20/08/2017	862	3.97	1.72	18.73	4.19	1.98	2.91	62.22	-	0.13	11	0.24	187
	27/08/2017	750	4.80	1.97	24.02	4.46	3.65	3.56	68.32	-	0.25	11	0.29	117
	04/09/2017	475	3.80	1.82	24.77	4.27	3.02	3.03	65.88	-	0.14	11	0.31	107
	10/09/2017	514	3.83	1.58	25.53	4.98	2.29	3.56	68.32	-	0.14	12	0.33	66
	17/09/2017	2910	3.42	1.80	15.36	2.95	3.02	2.98	37.82	4.14	0.18	9	0.30	343
	18/09/2017	2625	6.42	1.80	18.03	2.48	5.34	2.29	50.02	5.28	0.20	10	0.22	369
	24/09/2017	750	5.26	2.17	17.98	4.73	3.59	4.11	53.68	3.68	0.13	12	0.28	85
	01/10/2017	690	5.16	1.91	27.33	5.17	4.23	3.72	75.64	2.57	0.15	12	0.28	95
	08/10/2017	2045	4.43	2.09	17.08	3.16	3.81	2.89	46.36	4.61	0.20	9	0.26	75
	10/10/2017	3150	2.58	2.17	15.29	2.60	2.58	3.10	36.60	4.08	0.25	8	0.29	200
	12/10/2017	4422	2.88	2.07	15.99	2.65	2.47	2.90	51.20	4.10	0.20	10	0.13	186
	22/10/2017	735	5.53	1.63	25.39	4.72	3.01	4.19	65.88	3.34	0.16	13	0.32	56
	05/11/2017	480	5.65	1.65	27.58	5.57	3.02	4.31	73.20	2.93	0.12	13	0.33	18
	12/11/2017	420	6.03	1.84	26.64	5.22	3.54	3.56	82.96	2.63	0.14	13	0.24	22
	20/11/2017	400	4.44	1.22	25.01	4.56	2.88	4.37	67.01	2.38	0.15	13	0.29	17
	27/11/2017	327	3.86	1.45	22.46	4.69	1.81	3.25	58.56	2.64	0.15	13	0.34	7
	03/12/2017	375	8.50	2.00	21.65	6.42	6.69	4.70	69.54	4.58	0.12	12	0.26	4
	10/12/2017	260	5.61	1.71	24.48	5.69	3.42	4.34	57.34	3.52	0.10	13	0.40	13
	18/12/2017	326	5.79	2.14	24.39	5.38	4.50	5.03	69.54	2.72	0.09	13	0.28	10
	24/12/2017	287	7.04	1.84	24.89	6.65	3.79	4.48	76.86	4.08	0.07	13	0.29	6
	31/12/2017	255	4.60	1.68	26.27	5.37	2.64	3.80	74.42	2.26	0.13	12	0.29	13
	21/01/2018	310	6.72	1.45	28.38	8.43	2.63	5.37	95.20	1.18	0.12	12	0.27	5
	27/01/2018	235	7.45	3.49	27.94	6.19	2.88	3.85	64.66	2.05	0.04	11	0.46	9
	04/02/2018	275	8.30	2.09	28.76	6.84	5.80	5.67	73.20	3.77	0.12	11	0.36	6
	04/03/2018	260	4.18	1.73	27.21	5.33	2.38	4.35	78.08	2.23	0.03	12	0.27	3
	11/03/2018	180	4.89	2.18	30.04	6.16	3.30	4.87	78.08	4.76	0.08	11	0.32	23
	02/04/2018	148	10.15	2.34	30.54	7.58	7.63	5.80	57.30	2.97	0.06	11	0.50	14
	07/04/2018	120	5.21	1.58	30.06	6.55	2.68	4.24	82.96	2.09	0.11	12	0.32	18
	17/04/2018	142	4.72	1.85	29.25	6.25	1.88	4.05	73.20	1.92	0.20	13	0.38	7
	06/05/2018	119	8.91	2.17	23.71	5.69	6.59	4.78	62.22	5.48	0.25	11	0.33	211
	13/05/2018	335	6.60	2.05	27.64	5.50	4.01	4.61	73.20	3.64	0.25	12	0.32	55
	20/05/2018	180	5.29	2.87	27.21	5.81	2.66	5.58	62.00	2.82	0.21	12	0.41	33
	28/05/2018	176	7.10	2.30	31.14	7.70	3.69	8.85	93.94	2.04	0.22	10	0.27	25
	02/06/2018	149	5.22	2.05	27.49	5.51	2.62	3.80	74.42	2.13	0.25	12	0.33	13
	17/06/2018	240	11.81	3.21	28.47	8.15	9.51	8.73	73.20	3.16	0.21	13	0.36	12
	24/06/2018	370	5.07	1.78	24.02	5.48	2.26	4.20	75.64	0.90	0.11	12	0.26	24
	08/07/2018	300	5.25	2.16	28.80	6.26	2.44	4.28	81.74	1.28	0.25	12	0.32	52
	16/07/2018	350	3.35	1.82	22.31	4.34	2.93	5.47	65.88	1.70	0.09	10	0.21	246
	22/07/2018	1410	2.32	1.24	18.13	3.27	1.37	5.56	54.90	5.95	0.13	10	0.12	228

5.4.2. Spatial and seasonal variations of major solutes and suspended solids

The total concentrations of major solutes at My Ly ranged from 142 to 205 mg/L, averaging 168 mg/L. At Dua, TDS varied from 85 to 171 mg/L, averaging 138 mg/L. On the other hand, the TDS value at Yen Thuong ranged from 77 to 167 mg/L, averaging 128 mg/L. Generally, the total solute concentration decreased from upstream to downstream, consistent with decreased concentrations of the major ions Ca^{2+}, Mg^{2+}, Na^{+}, Cl^{-}, HCO_3^{-}, SO_4^{2-}, and SiO_2 in the downstream basin. The observed spatial variations in solute concentrations in the main stream of the Ca River could be related to the effects of tributary inflows, resulting in dilution. A significant downstream trend in K^{+} concentration was not significant, reflecting its

conservative behavior in the basin. An increase in NO_3^- concentration in the downstream basin might have been from anthropogenic sources such as agricultural activity and untreated sewage (Maharana et al. 2015).

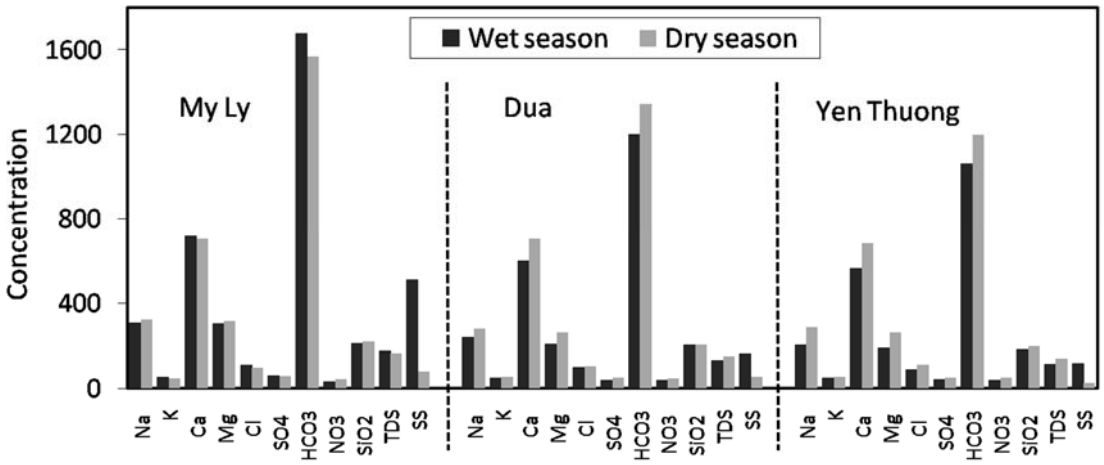

Figure 5.2. Seasonal variations in the concentration of major ions (µM), TDS, and SS (mg/l)

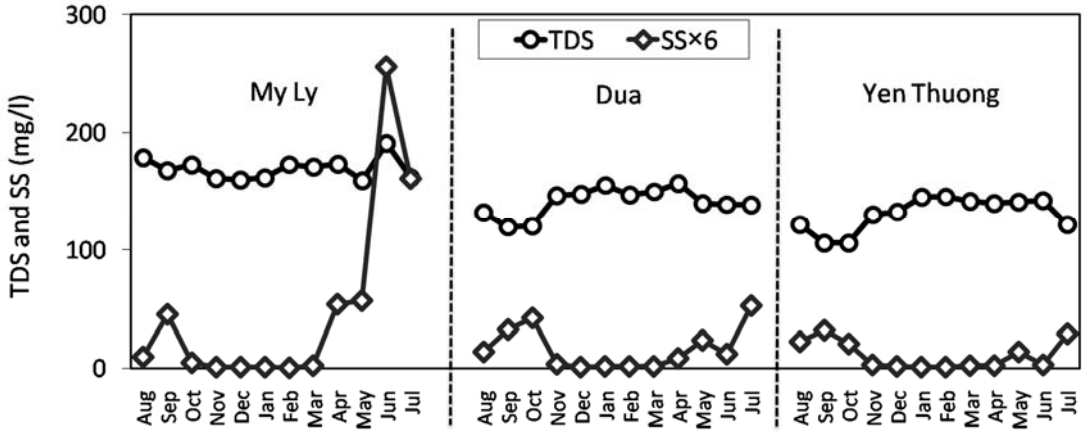

Figure 5.3. Monthly variations in the concentration of TDS and SS (mg/l)

The study period was divided into two sub-periods: the wet season (June to November for Dua and Yen Thuong and May to October for My Ly) and the dry season (December to May and November to April, respectively) (Figure 5.2). Trends in seasonal solute variations were similar between Dua and Yen Thuong. The concentrations of almost all tested ions increased from the wet to dry seasons, indicating the dilution effect of greater atmospheric precipitation during the rainy season. For that reason, at Dua and Yen Thuong, the total solute concentration increased from the wet to dry seasons. At My Ly, however, TDS decreased slightly from the wet to dry seasons, a result of decreased concentration in the major ion HCO_3^-. Other elements remained constant when comparing the two seasons. Phosphate

concentration increased in the wet season at all stations, indicating the contribution of organic matter degradation (at My Ly) or human activity (at Dua and Yen Thuong).

Normally, suspended sediment concentration (SSC) decreases from upstream to downstream and from the wet to dry seasons (Figure 5.2). In our case, it greatly varied from month to month (Figure 5.3), showing the opposite trend of that seen for solute concentration, except at My Ly (for example, in June and July). The highest SSCs occurred during September, October, and July at Dua and Yen Thuong (135–317 mg/L). Peak SSC occurred in June at My Ly (1534 mg/L), indicating significant erosion in the upper basin due to a heavy rain.

5.4.3. Weathering processes controlling the major ion chemistry

Major natural processes determining the ion chemistry of water can be identified by plotting variations in the weight ratio between Na^+ and $Na^+ + Ca^{2+}$ as a function of TDS (Gibbs 1970). The sources of major ions were divided into three groups: precipitation dominance, rock dominance, and evaporation-crystallization dominance. Figure 5.4 shows weathering dominance for most the samples drawn. Rock weathering controls the water composition in the Ca River basin, producing a TDS value between 77 and 205 mg/L and a $Na^+/(Na^+ + Ca^{2+})$ ratio ranging from 0.10 to 0.43.

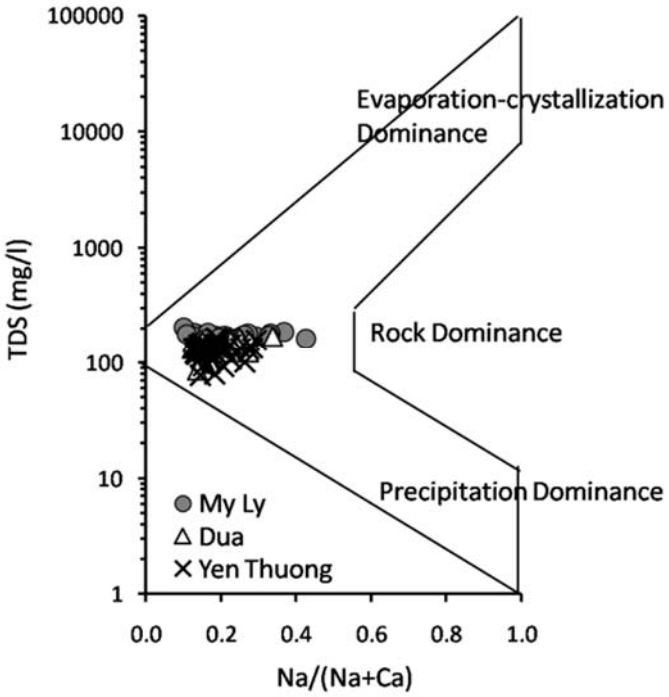

Figure 5.4. The Gibbs graph of Ca River between the ratio of Na/(Na+Ca) and total dissolved solids

Table 5.2. Correlation matrix of measured parameters at three hydrological stations

	Na^+	K^+	Ca^{2+}	Mg^{2+}	Cl^-	SO_4^{2-}	HCO_3^-	NO_3^-	PO_4^{3-}	SiO_2	TDS	TSS
My Ly												
Na^+	1.00											
K^+	0.43**	1.00										
Ca^{2+}	-0.30	0.16	1.00									
Mg^{2+}	0.26	0.11	0.48**	1.00								
Cl^-	0.91**	0.54**	-0.30	0.11	1.00							
SO_4^{2-}	0.44**	0.33*	0.04	0.05	0.46**	1.00						
HCO_3^-	-0.19	0.10	0.42**	0.30	-0.13	-0.04	1.00					
NO_3^-	0.49**	0.34	-0.17	-0.04	0.67**	0.24	-0.25	1.00				
PO_4^{3-}	-0.15	0.27	0.40*	0.01	-0.10	0.12	0.06	0.00	1.00			
SiO_2	0.12	0.17	0.01	0.17	-0.03	0.15	-0.19	-0.16	-0.04	1.00		
TDS	0.33*	0.49**	0.54**	0.55**	0.37*	0.34*	0.76**	0.18	0.15	-0.03	1.00	
TSS	-0.27	0.28	0.43**	-0.01	-0.12	0.23	0.35*	0.13	0.44**	-0.07	0.36*	1.00
Dua												
Na^+	1.00											
K^+	0.68**	1.00										
Ca^{2+}	0.45**	0.25	1.00									
Mg^{2+}	0.64**	0.47**	0.85***	1.00								
Cl^-	0.89**	0.56**	0.22	0.37*	1.00							
SO_4^{2-}	0.67**	0.77**	0.46**	0.68**	0.41**	1.00						
HCO_3^-	0.31*	0.03	0.78**	0.65**	0.16	0.33*	1.00					
NO_3^-	0.35*	0.49**	-0.47**	-0.10	0.39*	0.28	-0.47**	1.00				
PO_4^{3-}	-0.30	0.00	-0.35*	-0.39*	-0.20	-0.30	-0.48**	0.13	1.00			
SiO_2	0.35*	0.06	0.28	0.43**	0.19	0.32*	0.45**	-0.03	-0.41**	1.00		
TDS	0.69**	0.40**	0.86**	0.86**	0.50**	0.62**	0.88**	-0.19	-0.49**	0.51**	1.00	
TSS	-0.42**	-0.10	-0.59**	-0.53**	-0.25	-0.18	-0.66**	0.28	0.49**	-0.53**	-0.66**	1.00
Yen Thuong												
Na^+	1.00											
K^+	0.56**	1.00										
Ca^{2+}	0.50**	0.23	1.00									
Mg^{2+}	0.73**	0.34*	0.84**	1.00								
Cl^-	0.87**	0.50**	0.19	0.41**	1.00							
SO_4^{2-}	0.60**	0.39*	0.53**	0.71**	0.49**	1.00						
HCO_3^-	0.25	-0.09	0.76**	0.70**	-0.06	0.40**	1.00					
NO_3^-	0.02	-0.03	-0.55**	-0.45**	0.31	-0.16	-0.58**	1.00				
PO_4^{3-}	-0.08	0.09	-0.19	-0.24	0.02	-0.06	-0.12	0.16	1.00			
SiO_2	0.29	-0.13	0.55**	0.51**	0.04	0.15	0.54**	-0.41*	-0.23	1.00		
TDS	0.59**	0.16	0.90**	0.89**	0.28	0.63**	0.92**	-0.48**	-0.15	0.59**	1.00	
TSS	-0.37*	-0.17	-0.72**	-0.72**	-0.07	-0.36*	-0.60**	0.51**	0.30	-0.69**	-0.69**	1.00

**Correlation is significant at the 0.01 level
*Correlation is significant at the 0.05 level

The three primary lithologies undergoing chemical weathering were silicates, carbonates, and evaporites (Gaillardet et al. 1997). Carbonate weathering (calcite, dolomites) produces Ca^{2+}, Mg^{2+}, and HCO_3^-. Silicate weathering results in HCO_3^-, Na^+, K^+, Mg^{2+}, Ca^{2+}, and SiO_2. Evaporite dissolution results in Na^+, K^+, Cl^-, and SO_4^{2-} (Han and Liu 2001; Meybeck 1987; Sarin et al. 1989). The relationships between Ca^{2+}/HCO_3^-, $(Ca^{2+} + Mg^{2+})$/total cations, and $(Na^+ + K^+)$/total cations for the Ca River were determined to evaluate the contribution of rock weathering. The Ca^{2+}andHCO_3^- for most samples fell along a 1:1 equiline (Figure 5.5a), implying that carbonates dissolution dominates in this drainage basin (Roy et al. 1999). The HCO_3^- is slightly more enriched than Ca^{2+}at My Ly, possibly consistent with a silicate weathering source for some of this anion (Holland 1978). The scatter plot (Figure 5.5b) of $Ca^{2+} + Mg^{2+}$)against total cations indicates a significant contribution these two cations (approximately 85% of the total). Any deviation of $Ca^{2+} + Mg^{2+}$) from the

1:0.85 line was attributed to increasing proportions of $Na^+ + K^+$) (Figure 5.5b and 5.5c), implying contributions from silicate weathering or evaporite dissolution (Li and Zhang 2008; Maharana et al. 2015). The correlations among geochemistry parameters and their correlations with suspended solids was investigated for each station (Table 5.2). The significant relationships between Ca^{2+}/Mg^{2+}, Ca^{2+}/HCO_3^-, Mg^{2+}/HCO_3^-, Ca^{2+}/TDS, Mg^{2+}/TDS, and HCO_3^-/TDS at all stations support the finding of carbonate weathering dominance in the Ca River basin. Significant correlations between SiO_2 and Na^+, K^+, or HCO_3^- were not found, implying minimal silicate weathering. However, moderate correlations between Cl^-, SO_4^{2-}, Na^+, K^+, and TDS were found, indicating that evaporite weathering was the source (Li and Zhang 2008).

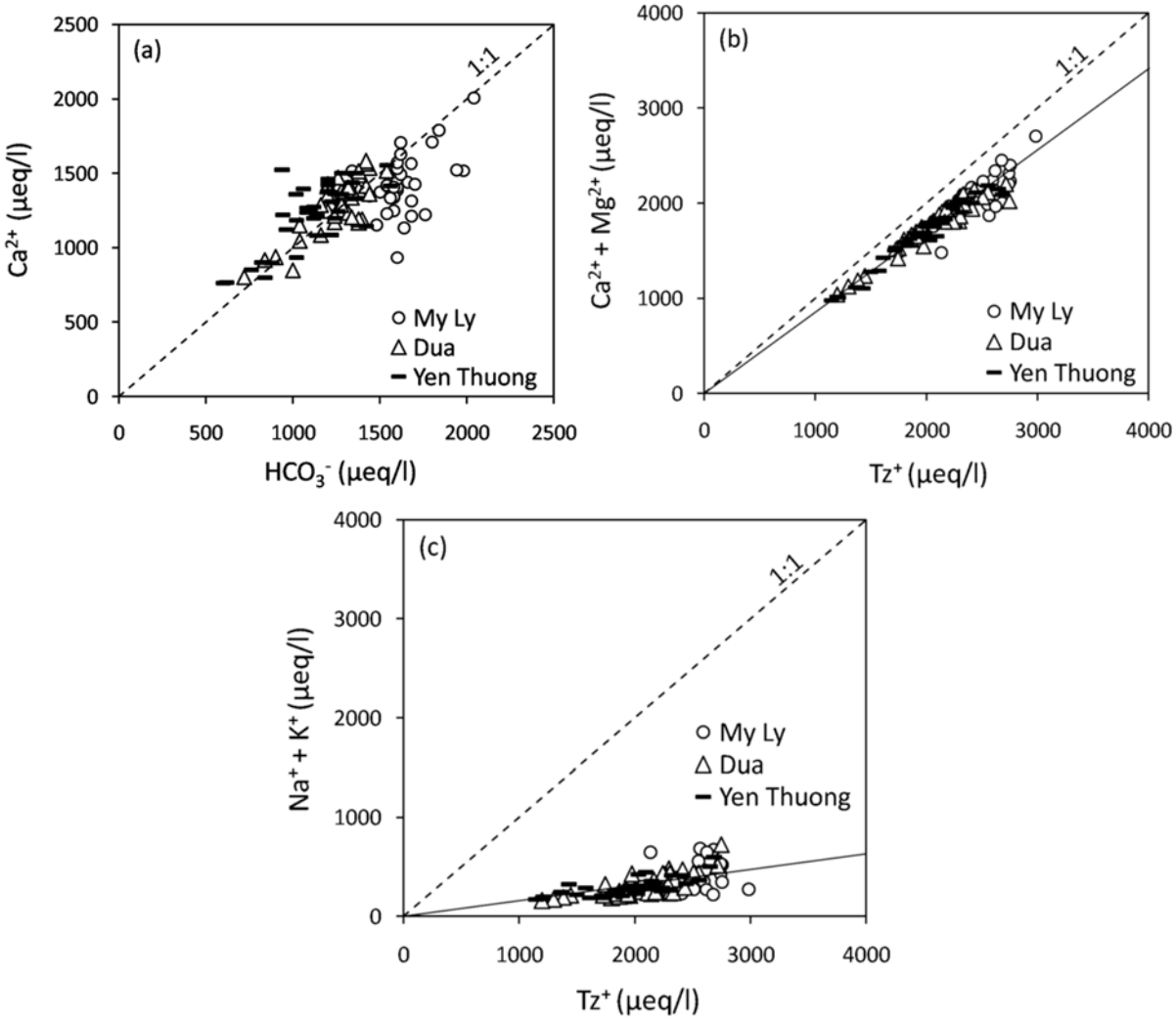

Figure 5.5. Scatter plots between (a) Ca^{2+} and HCO_3^-, (b) Ca^{2+}, Mg^{2+}, and total cations, and (c) Na^+, K^+, and total cations

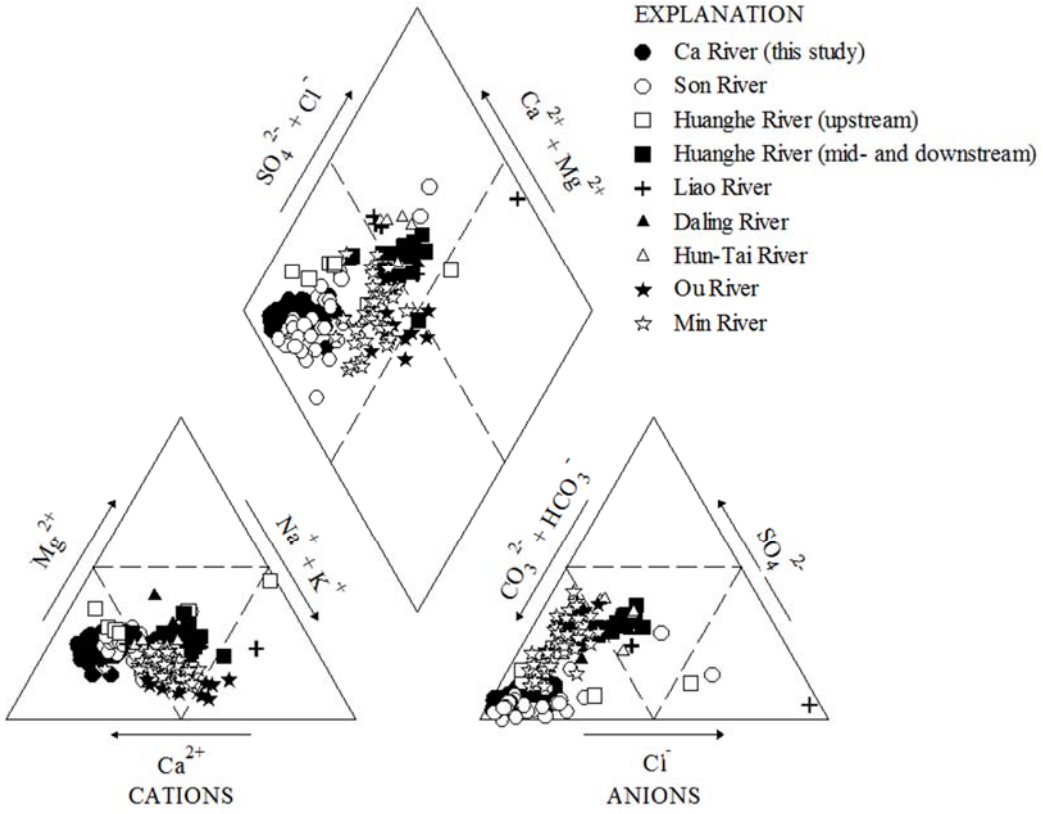

Figure 5.6. Piper trilinear diagram of Ca River water in comparison with other river basins (data from Ding et al. 2016; Fan et al. 2014; Liu et al. 2018; Maharana et al. 2015)

The Piper diagram is widely applied to determine the classification of water on the basis of its chemical character (Maharana et al. 2015; Negrel et al. 2007; Ji and Jang 2012). The triangular cationic fields of the Piper diagram (Figure 5.6) revealed that most of the water samples fell into the Ca^{2+} field, whereas in the anion triangle, the majority fell into the HCO_3^- field. Chemical data plotted on the diamond-shaped central field revealed the dominance of the $Ca^{2+} - HCO_3^-$ type. Therefore, $Ca^{2+} - HCO_3^-$ is the dominant hydrogeochemical species in the Ca River basin. The Piper diagram for our Ca River samples is similar to that for the Son River (Maharana et al. 2015) and the upstream Huanghe River (Fan et al. 2014), dominated by carbonate weathering. However, it differs from the mid- and downstream sections of the Huanghe River (Fan et al. 2014), where evaporite dissolution dominates. They also differ from the Liao River, Daling River, Hun-Tai River (Ding et al. 2016), Ou River, and Min River (Liu et al. 2018), where silicate weathering dominates. In many watersheds around the world, carbonate weathering plays important roles in controlling river water chemistry because carbonate is more susceptible to weathering than silicate (Fan et al. 2014; Roy et al. 1999).

5.4.4. Variations of major solute concentration with discharge

The relationships between solute concentration and its discharge were investigated at each hydrological station. Concentrations of the weathering-derived solutes were plotted against instantaneous discharge on logarithmic axes (Figure 5.7), yielding the approximate relationships between concentration and discharge using a power law (Baronas et al. 2017; Herndon et al. 2015; Musolff et al. 2015):

$$C = a \times Q^b \tag{5.1}$$

where C is solute concentration, Q is discharge, and a and b are constants. The exponent b is the slope of the $C - Q$ relationship on logarithmic axes. When concentration does not change with changing discharge, the relationship is said to be chemostatic (Moatar et al. 2017; Musolff et al. 2015). When this is the case, b is between -0.1 and 0 (Herndon et al. 2015; Hunsaker and Johnson 2017). When discharge increases, solute concentrations can either increase (enrichment behavior, $b > 0$) or decrease (dilution behavior, $b < -0.1$), and the relationship is said to be chemodynamic (Herndon et al. 2015).

Our results show that the upstream catchment (My Ly) behaved chemostatically for the major chemical weathering products except Na^+ ($b = -0.11$), NO_3^- ($b = 0.11$), and PO_4^{3-}($b = 0.15$). The large store/high production rate of weathering products can lead to chemostatic behavior for major ions (Musolff et al. 2015). Nutrient increases with increasing discharge at My Ly indicated the source was organic matter degradation in the forest area. Similar trends for the major ions at discharge were seen at Dua and Yen Thuong. Negative slopes were found for Ca^{2+}, Mg^{2+}, and HCO_3^- ($b = -0.12\ to\ -0.28$) with low variability ($R^2 \geq 0.5$) and for Na^+ and SO_4^{2-} ($b = -0.13\ to\ -0.22$) with moderate variability ($R^2 \geq 0.3$). The concentrations of NO_3^- and PO_4^{3-} were constant or increasing, indicating enrichment in nutrient sources in the basin (Musolff et al. 2015). Meanwhile, K^+ and Cl^- behaved chemostatically, increasing in the discharge at all basins, indicating important biogeochemical influences (Saunders and Lewis 1989) or exogenous sources (atmospheric deposition) (Musolff et al. 2015). For the major solutes (Ca^{2+}, Mg^{2+}, Na^+, and HCO_3^-), the dilution slopes at the downstream station were greater than those found midstream, indicating that catchments with higher water yields were more likely to express dilution (Moatar et al. 2017). The negative correlation between major elements and runoff increased (higher R^2 values) with decreasing elevation (Torres et al. 2015). Less-reactive elements (Ca^{2+}, Mg^{2+}, and HCO_3^-) exhibited strong correlations with discharge and indicated various degrees of dilution with increasing runoff (Baronas et al. 2017). However, low correlations found for PO_4^{3-}, NO_3^-,

Cl^-, and K^+ reflected biological processes, atmospheric input, or anthropogenic impacts (i.e., fertilizer application) (Bluth and Kump 1994; Moatar et al. 2017).

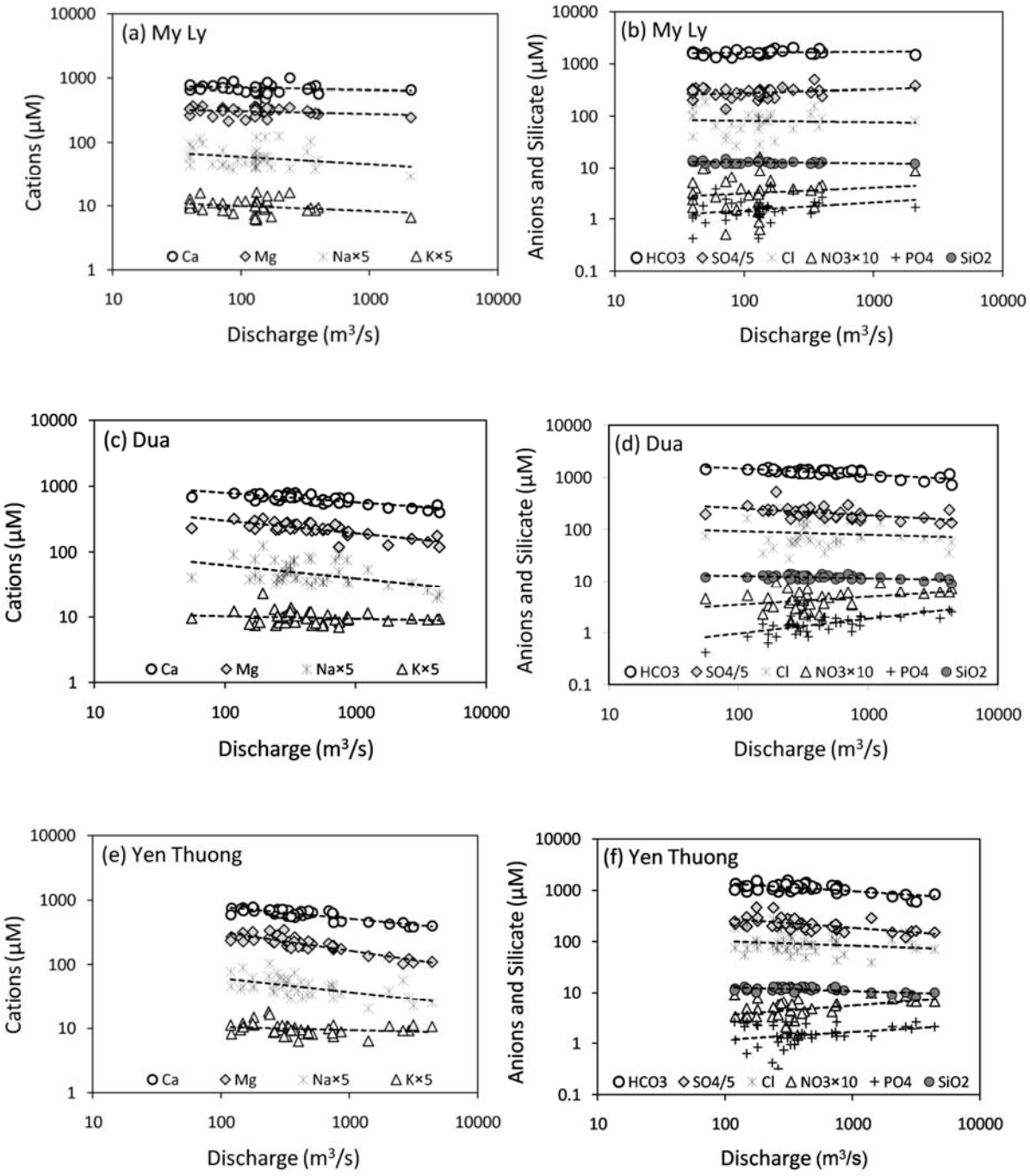

Figure 5.7. Variation of river elements concentration with discharge at My Ly (a, b), Dua (c, d), and Yen Thuong (e, f)

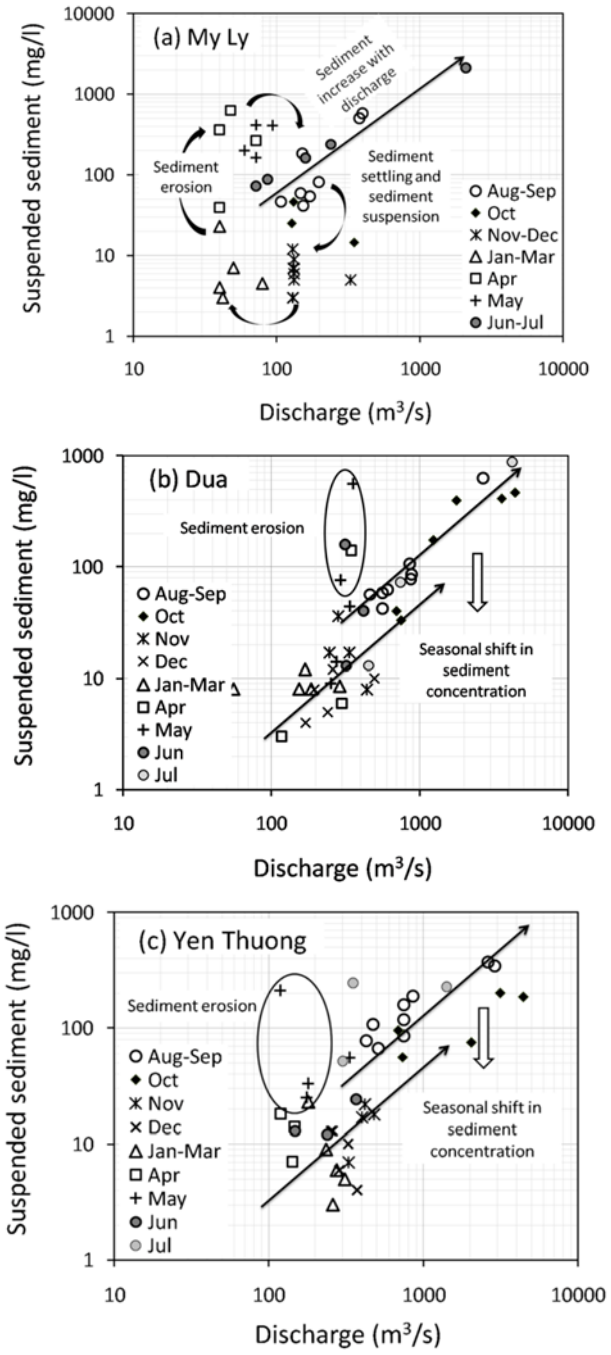

Figure 5.8. Variation of suspended sediment concentration with discharge at My Ly (a), Dua (b) and Yen Thuong (c)

5.4.5. Primary evidence of reservoir impact on suspended solids and dissolved solids concentration

Located above the largest reservoir of the Ca River basin, My Ly is significantly influenced by the operation of the Ban Ve reservoir. The impact of water storage at the Ban Ve reservoir on the correlation between SSC and discharge at My Ly is shown in Figure 5.8a. In August and September (rainy season), SSC increased with increasing discharge. Water

storage starts at the end of the rainy season (October), leading to increased water levels behind the reservoir. The water level was raised until it was over the My Ly station. Consequently, runoff was delayed during November and December. As a result, the SSC gradually decreased as suspended sediment settled, and sediment suspension was deferred during this period. The reservoir opened at the beginning of January, but SSC remained low until March because it was the dry season. Rain in April and May can wash out the settled sediment surrounding the upper part of My Ly, resulting in the steep increases in SSC. Thereafter, SSC increases with increasing discharge in June and July, consistent with increases seen in August and September.

Dua and Yen Thuong, located in the lower part of the main reservoirs in the Ca River basin, showed similar SSC behaviors in their discharges (Figures 5.8b and 5.8c): decreasing SSCs with increasing discharge when comparing the rainy to dry seasons. This reflects the impact of suspended sediment settling in the reservoirs. Upstream sediment erosion also influenced that seen downstream; this is implied by the high SSC found in May. Generally, SSCs are positively correlated with streamflow (Moore and Anderholm 2002). However, reservoir operations lead to a variety of SSC behaviors in the discharge.

Dam closure not only affects suspended sediment but also river water quality (Muigai et al. 2010; Castilla-Hernandez et al. 2014). Variations in solute concentrations with discharge at My Ly were quite different from the fluxes with discharge at Dua and Yen Thuong. Differences could be the results of impacts of the reservoir. During the wet season, when water is stored at My Ly, most ion concentrations were less variated than in other periods. When the reservoir was open, ion concentrations increased with discharge during the dry season until the highest concentration was reached at the first flash flood on 17 June 2018. Since then, ion concentrations decreased due to dilution. However, inverse correlations between ion concentrations and discharges were seen at Dua and Yen Thuong, indicating dilution effects (Zhang et al. 2015). When discharge exceeded 1000 m^3/s, ion concentrations decreased sharply, for example, on 17 December 2017, 8–12 October 2017, and 22 July 2018. The correlations between TSS and geochemical parameters are shown in Table 2 and indicate that suspended solids are negatively correlated with all ions (except $NO_3^-$and PO_4^{3-}) and TDS at Dua and Yen Thuong. This is common with increases in sediment, whereas chemical ions become diluted with increasing discharge. In contrast, positive correlations between TSS and K^+, Ca^{2+}, SO_4^{2-}, HCO_3^-, NO_3^-, PO_4^{3-}, and TDS were identified at My Ly. These results imply a significant geochemical impact of water storage in the My Ly basin. When the water level at

My Ly rises, My Ly can act as a reservoir, resulting in sediment suspension and sediment settling. Dam closures lead to increased water residence time, causing increased interaction between sediment particles and solutes. Dam closures also change the environmental water conditions (low oxygen content and high temperature), favoring biogeochemical processes (Moatar et al. 2017). Muigai et al. (2010) indicated that the reservoir leads to decreases in dissolved oxygen content due to eutrophication and increases the TDS value. Moore and Anderholm (2002) found that, in downstream reservoirs, TDS concentrations increase from evapotranspiration while nutrient concentrations decrease from settling and nutrient uptake, and SSCs decrease due to settling. In this study, it was not easy to assess the impact of the reservoir on the downstream basin because TDS values showed small seasonal variations. Moreover, the TDS concentration and composition were significantly influenced by multiple factors such as human activity, groundwater discharge, and tributary inflow. Therefore, the impact of dam closure on TDS in the downstream basin requires further investigation.

5.6. CONCLUSIONS

From 121 Ca River water samples collected from August 2017 to July 2018 at three stations, cation (Ca^{2+}, Mg^{2+}, Na^{+}, and K^{+}), anion (HCO_3^-, SO_4^{2-}, Cl^-, NO_3^-, and PO_4^{3-}), dissolved silica, SSCs, and TDS values showed that carbonate weathering is dominant. Bicarbonate and calcium are the prevailing chemical species, accounting for 84.4% and 62.0% of the total anionic and cationic charges, respectively. The TDS values varied from 77 to 205 mg/L, averaging 144 mg/L and decreasing in the downstream basin with decreases in major solute concentrations.

The relationships between solute concentrations and discharge show that the upstream catchment (My Ly) behaves chemostatically for the major chemical weathering products. Similar negative trends for Ca^{2+}, Mg^{2+}, HCO_3^-, Na^{+}, and SO_4^{2-} with discharge at Dua and Yen Thuong indicate dilution behaviors for those ions. The constant or increasing ion concentrations of NO_3^- and PO_4^{3-} in the three basins reflect enrichment of nutrients from organic matter degradation or human activity.

Relationships between SSC and discharge show that the reservoirs along the Ca River trigger sediment suspension and sediment settling at the My Ly station and decreasing SSCs at the Dua and Yen Thuong stations. Delays in water flow can lead to greater interactions between sediment and solutes and can allow biogeochemical processes that result in unusual changes in the concentrations of major ions and TDS with increasing discharges at My Ly.

REFERENCES

Amos P, Veale B, Thai NC, Read S (2017) Improving dam and downstream community safety in Vietnam. Hydropower Dams 1: 37–43

Baronas JJ, Torres MA, Clark KE, West AJ (2017) Mixing as a driver of temporal variations in river hydrochemistry: 2. Major and trace element concentration dynamics in the Andes-Amazon transition. Water Resour Res 53(4): 3120–3145

Bluth GJS, Kump LR (1994) Lithologic and climatologic controls of river chemistry. Geochim Cosmochim Acta 58(10): 2341–2359

Bruijnzeel LA (1983) Hydrological and biogeochemical aspects of man-made forests in south-central Java, Indonesia. PhD Thesis, Vrije Universiteit, Amsterdam, 256 pp

Castilla-Hernandez P, Torres-Alvarado M del R, Herrera-San Luis JA, Cruz-Lopez N (2014) Water quality of a reservoir and its major tributary located in east-central Mexico. Int J Environ Res Public Health 11(6): 6119–6135

Chetelat B, Liu C-Q, Zhao ZQ, Wang QL, Li SL, Li J, Wang BL (2008) Geochemistry of the dissolved load of the Changjiang Basin rivers: Anthropogenic impacts and chemical weathering. Geochim Cosmochim Acta 72(17): 4254–4277

Chikamori H, Heng L, Daniel T (eds) (2012) Catalogue of rivers for Southeast Asia and the Pacific–Volume VI. UNESCO-IHP Regional Steering Committee for Southeast Asia and the Pacific. http://unesdoc.unesco.org/images/0021/002170/217039e.pdf

Ding H, Liu C-Q, Zhao Z-Q, Li S-L, Lang Y-C, Li X-D, Hu J, Liu B-J (2016) Geochemistry of the dissolved loads of the Liao River basin in northeast China under anthropogenic pressure:Chemical weathering and controlling factors. J Asian Earth Sci 138: 657–671

Fan B-L, Zhao Z-Q, Tao F-X, Liu B-J, Tao Z-H, Gao S, Zhang L-H (2014) Characteristics of carbonate, evaporite and silicate weathering in Huanghe River basin: A comparison among the upstream, midstream and downstream. J Asian Earth Sci 96: 17–26

Gaillardet J, Dupre B, Allegre CJ, Negrel P (1997) Chemical and physical denudation in the Amazon River Basin. Chem Geol 142(3–4): 141–173

Gibbs RJ (1970) Mechanisms controlling world water chemistry. Science 170(3962): 1088–1090

Godsey SE, Kirchner JW, Clow DW (2009) Concentration–discharge relationships reflect chemostatic characteristics of US catchments. Hydrol Process 23(13): 1844–1864

Han G, Liu C (2001) Hydrogeochemistry of Wujiang River water in Guizhou province China. Chin J Geochem 20(3): 240–248

Herndon EM, Dere AL, Sullivan PL, Norris D, Reynolds B, Brantley SL (2015) Landscape heterogeneity drives contrasting concentration–discharge relationships in shale headwater catchments. Hydrol Earth Syst Sci 19: 3333–3347

Holland HD (1978) The chemistry of the atmosphere and oceans. John Wiley & Sons, 351 pp

Hunsaker CT, Johnson DW (2017) Concentration-discharge relationships in headwater streams of the Sierra Nevada, California. Water Resour Res 53(9): 7869–7884

IWRP (2012) Synthesis report of "Review of water resources planning in the Ca River basin" (in Vietnamese). Institute of Water Resources Planning, Directorate of Water Resources, Ha Noi

Ji H, Jiang Y (2012) Carbon flux and C, S isotopic characteristics of river waters from a karstic and a granitic terrain in the Yangtze River system. J Asian Earth Sci 57: 38–53

Li S, Xu Z, Wang H, Wang J, Zhang Q (2009) Geochemistry of the upper Han River basin, China 3: Anthropogenic inputs and chemical weathering to the dissolved load. Chem Geol 264(1–4): 89–95

Li S, Zhang Q (2008) Geochemistry of the upper Han River basin, China, 1: Spatial distribution of major ion compositions and their controlling factors. Appl Geochem 23(12): 3535–3544

Liu W, Xu Z, Sun H, Zhao T, Shi C, Liu T (2018) Geochemistry of the dissolved loads of rivers in Southeast Coastal Region, China: Anthropogenic impact on chemical weathering and carbon sequestration. Biogeosciences Discuss

Maharana C, Gautam SK, Singh AK and Tripathi JK (2015) Major ion chemistry of the Son River, India: Weathering processes, dissolved fluxes and water quality assessment. J Earth Syst Sci 124(6): 1293–1309

Meybeck M (1987) Global chemical weathering of surficial rocks estimated from river dissolved loads. Am J Sci 287(5): 401–428

Meybeck M (1994) Origin and variable composition of present day riverborne material. In: Material Fluxes on the Surface of the Earth. Washington, DC, National Academic Press, pp 61–73

Meybeck M, Helmer R (1989) The quality of rivers: From pristine stage to global pollution. Palaeogeogr Palaeoclimatol Palaeoecol 75(4): 283–309

Milliman JD, Farnsworth KL (2011) River discharge to the coastal ocean: a global synthesis. Cambridge University Press, 384 pp

Moatar F, Abbott BW, Minaudo C, Curie F, Pinay G (2017) Elemental properties, hydrology, and biology interact to shape concentration-discharge curves for carbon, nutrients, sediment, and major ions. Water Resour Res 53(2): 1270–1287

Moon S, Huh Y, Qin J, Pho NV (2007) Chemical weathering in the Hong (Red) River basin: Rates of silicate weathering and their controlling factors. Geochim Cosmochim Acta 71(6): 1411–1430

Moore SJ, Anderholm SK (2002) Spatial and temporal variations in streamflow, dissolved solids, nutrients, and suspended sediment in the Rio Grande Valley study unit, Colorado, New Mexico, and Texas, 1993–95. US Geological Survey, National Water-Quality Assessment Program, Water-Resources Investigations Report 02-4224, Albuquerque, NM, 52 pp

Muigai PG, Shiundu PM, Mwaura FB, Kamau GN (2010) Correlation between dissolved oxygen and total dissolved solids and their role in the eutrophication of Nairobi dam, Kenya. Int J of BioChemiPhysics 18: 38–46

Musolff A, Schmidt C, Selle B, Fleckenstein JH (2015) Catchment controls on solute export. Adv Water Resour 86: 133–146

Nauditt A and Ribbe L (eds) (2017) Land use and climate change interactions in central Vietnam. Springer Book Series: Water Resources and Development

Negrel P, Roy S, Petelet-Giraud E, Millot R, Brenot A (2007) Long-term fluxes of dissolved and suspended matter in the Ebro River Basin (Spain). J Hydrol 342(3–4): 249–260

Roy S, Gaillardet J, Allegre CJ (1999) Geochemistry of dissolved and suspended loads of the Seine river, France: Anthropogenic impact, carbonate and silicate weathering. Geochim Cosmochim Acta 63(9): 1277–1292

Sarin MM, Krishnaswami S, Dilli K,Somayajulu BLK, Moore WS (1989) Major ion chemistry of the Ganga-Brahmaputra river system: Weathering processes and fluxes to the Bay of Bengal. Geochim Cosmochim Acta 53(5): 997–1009

Saunders JF, Lewis WM (1989) Transport of major solutes and the relationship between solute concentrations and discharge in the Apure River, Venezuela. Biogeochemistry 8(2): 101–113

Torres MA, West AJ, Clark KE (2015) Geomorphic regime modulates hydrologic control of chemical weathering in the Andes–Amazon. Geochim Cosmochim Acta 166: 105–128

White AF and Blum AE (1995) Effects of climate on chemical weathering in watersheds. Geochim Cosmochim Acta 59(9): 1729–1747

Xiao J, Jin Z-D, Ding H, Wang J, Zhang F (2012) Geochemistry and solute sources of surface waters of the Tarim River Basin in the extreme arid region, NW Tibetan Plateau. J Asian Earth Sci 54–55: 162–173

CHAPTER 6. CONCLUSIONS

The Ca River is the third largest river in Vietnam but an international basin. A number of dams has been constructed expecting those hydropower and water resources. This is the reason why the synoptic model to overview the river basin becomes important.

Synoptic model is based on a run-off model and associated by some hydrological, hydraulic, and statistical routines or formulas. A model to overview the river basin on runoff, water quality, and sediment transport is considered for given meteorological condition. A hydrological tank model with optimized parameters is used to withdraw anthropogenic influences in Chapter 3. The river regime law and resistance law were simulated into the estimation of suspended sediment load in Chapter 4. The sediment load obtained from regime laws was favorably compared with existing methods. The transport of suspended sediment and dissolved matters were calculated by applying loading curve in Chapter 4 and 5. The results of synoptic model indicate the significant impact of human activities on discharge and material fluxes of the tributary and main stream of the Ca River.

Chapter 3, 4 and 5 contain their own conclusions, which are related to runoff, sediment and geochemistry.

The synoptic model provides a stable, multi-parametric and explicit procedure, which contributes to give feasible solutions for regional environmental issues including long-term and socio-economic aspects.

ACKNOWLEDGEMENTS

I would like to express my deepest gratitude to my advisor, Professor Kenji Okubo, for his guidance, patience, caringand providing me with an excellent atmosphere for doing research. I would like to thank my co-advisors, ProfessorMd. Azhar Uddin and Professor Hidetaka Chikamori for their greatsupports and suggestions on my study.

I also would like to express my deep appreciation to Dr. Mitsuyo Saito of the Graduate School Environmental and Life Science, Okayama University for her helpful comments pertaining to the manuscript and kind support throughout the research process. I am also grateful to Mr. Fabian Paliken for his comments that greatly improved the quality of the manuscript submitted to Asian Journal of Water, Environment and Pollution. I also thank Nguyen Xuan Tien of North-Central Hydro-meteorological Centre, Vietnam and the staff at the My Ly, Dua and Yen Thuong hydrological stations for allowing me to access their gauging records.

In addition, I would like to thank all my colleagues in the Environmental Department of Vinh University for their helps, kind supports and encouragement. I would also like to thank all my colleagues in the Laboratory of Professor Kenji Okubo, Graduate School of Environmental and Life Science, Okayama University for their experimental instructions and helping me to overcome language barrier during my stay in Japan. I would like to thank my students in Vinh University, especially to Nguyen Thi Tam, Dang Quoc Phong, Nguyen Thi Huyen and Tran Thi My Nhan for their helps in collection and analysis of river water samples.

I express my deep gratitude to my parents and all family membersfor their moral support and encouragement.

For financial support, I want to show my great appreciation to the Japan Society for the Promotion of Science (JSPS) RONPAKU (R11604) for supporting my research in Japan.

Ho Thi Phuong